Investigation of the adiabatic assumption for estimating cloud micro- and macrophysical properties from satellite and ground

D. Merk[1]**, H. Deneke**[1]**, B. Pospichal**[2]**, and P. Seifert**[1]

[1]Leibniz Institute for Tropospheric Research, Leipzig, Germany
[2]Leipzig Institute for Meteorology, Leipzig, Germany

Correspondence to: D. Merk (merk@tropos.de)

Abstract. Cloud properties from both ground-based as well as from geostationary passive satellite observations have been used previously for diagnosing aerosol-cloud interactions and specifically the Twomey effect. In this investigation, a two year dataset together with four selected case studies are analyzed with the aim of evaluating the consistency and limitations of current ground-based and satellite-retrieved cloud property datasets. The adiabatic cloud model is often applied and modified using a sub-adiabatic factor to account for entrainment within the cloud. Based on the adiabatic factor obtained from the combination of ground-based cloud radar, ceilometer and microwave radiometer, we demonstrate that neither the assumption of a completely adiabatic cloud nor the assumption of a constant sub-adiabatic factor is fulfilled (mean adiabatic factor 0.63 ± 0.22). As cloud adiabacity is required to estimate the cloud droplet number concentration, but is not available from passive satellite observations, an independent method to estimate the adiabatic factor, and thus the influence of mixing, would be highly desirable for global-scale analyses. Considering the radiative effect of a cloud described by the sub-adiabatic model, we focus on cloud optical depth and its sensitivities. Ground-based estimates are here compared versus cloud optical depth retrieved from the Meteosat SEVIRI satellite instrument resulting in a bias of -4 and a root mean square difference of 16. While synergistic methods based on the combination of ceilometer, cloud radar and microwave radiometer enable an estimate of the cloud droplet concentration, it is highly sensitive to radar calibration and to assumptions about the moments of the droplet size distribution. Similarly, satellite-based estimates of cloud droplet concentration are uncertain. We conclude that neither the ground-based nor satellite-based cloud retrievals applied here allow a robust estimate of cloud droplet concentration, which complicates its use for the study of aerosol-cloud interactions.

1 Introduction

Low-level liquid clouds play an important role in the energy balance of the Earth, and are found in many areas around the globe. Their microphysical and optical properties are strongly influenced by aerosol particles that act as cloud condensation nuclei. Twomey (1974) first postulated the effect of an increased aerosol number concentration in clouds on the radiative budget, commonly referred to as the first indirect aerosol effect, as a climatically relevant process. The quantification of such aerosol indirect effects remains one of the main uncertainties in climate projections (Boucher et al., 2013). If the liquid water content as well as the geometrical depth of the cloud are considered constant, a higher aerosol load results in an enhanced cloud albedo. This effect is observed in particular by means of ship tracks that form in marine stratocumulus cloud decks (e.g. Ackerman et al., 2000).

Cloud quantities that are typically used to calculate aerosol-cloud interactions, are the cloud droplet number concentration (N_d) and cloud geometrical depth (H). Brenguier et al. (2000) noted that a 15 % change in H can have a similar effect on cloud albedo as a doubling of N_d. Han et al. (1998) proposed to investigate a column N_d which is a combination with H.

While remote sensing observations from ground are always column measurements, passive satellite observations from e.g., SEVIRI or MODIS, show a good tradeoff in terms of spatio-temporal coverage, and are therefore suitable to investigate the first indirect aerosol effect on a larger scale. Active satellite sensors on the other hand, such as the cloud profiling radar onboard CloudSat (Stephens et al., 2002) or the Cloud-Aerosol-Lidar with Orthogonal Polarization (CALIOP) on-board CALIPSO (Winker et al., 2009,

Cloud-Aerosol Lidar and Infrared Pathfinder Satellite Observation), are able to provide vertically resolved cloud observations along their tracks and can be used to investigate aerosol effects on cloud properties (e.g. Christensen and Stephens, 2011). These lack highly-resolved temporal coverage and have a smaller scanning swath than passive sensors onboard polar-orbiting satellites. Despite their coarser spatial resolution, geostationary satellite observations benefit from the high temporal coverage of up to 5 minutes in conjunction with a high spatial coverage. This can be considered as an advantage for the determination of large-scale aerosol-cloud interactions, since the full daily cycle can be obtained and contrasted to ground-based observations.

If entrainment in clouds leads to a deviation from a linear increasing liquid water content, i.e. sub-adiabatic clouds, the first aerosol effect is not easily observed (Kim et al., 2008). To obtain key quantities from passive satellite observations, the sub-adiabatic cloud model is usually applied (e.g. Schueller et al., 2003; Boers et al., 2006; Bennartz, 2007). Therefore obtaining cloud adiabacity is important for the investigation of aerosol-cloud interactions. The combination of ground-based ceilometer and cloud radar is able to provide reliable detection of cloud geometric borders (Boers et al., 2000; Shupe, 2007; Illingworth et al., 2007; Martucci et al., 2010). N_d from ground-based observations can be retrieved from radar-radiometer measurements (Frisch et al., 1995), observations including including lidar measurements (Schmidt et al., 2014; Martucci and O'Dowd, 2011), or solar radiation measurements (Dong et al., 1997, 2002). To derive N_d from radar-radiometer observations Rémillard et al. (2013) recently suggested a condensational growth model taking the vertical velocity into account and allowing small variations of N_d with height, while it is assumed vertically constant in most other studies. Due to the underconstrained nature and assumptions made in such retrieval methods, substantial differences for the microphysical properties may occur, as pointed out by Turner et al. (2007), who intercompared several ground-based retrieval methods for one case study. Brandau et al. (2010) showed that the cloud optical depth is less sensitive to the assumptions required in radar-radiometer retrieval approaches and might be considered as an alternative key quantity.

As a consistency check, we contrast key quantities from ground-based remote sensing using a ceilometer, a microwave radiometer and a 35-GHz cloud radar at Leipzig, Germany (51.35 N, 12.43 E) and at Krauthausen, Germany (50.897 N, 6.46 E) with observations from SEVIRI (Spinning Enhanced Visible and InfraRed Imager) onboard Meteosat Second Generation (MSG). Those ground-based instruments are operated in the framework of Cloudnet (Illingworth et al., 2007) and ACTRIS (Aerosols, Clouds and Trace gases Research InfraStructure Network). To our knowledge such evaluations from the SEVIRI instrument for key parameters have been rarely carried out (e.g. in Roebeling et al., 2008b). Thereby, we discuss the uncertainties introduced by required assumptions when cloud microphysical properties are retrieved, and the effect of different spatio-temporal resolution. As the sub-adiabatic cloud model is a key concept for the retrievals discussed in this study, we aim to quantify cloud adiabacity using the available observations.

The paper is structured as follows. In Sect. 2 we introduce the sub-adiabatic model, relevant for the satellite-based retrieval of key parameters, as well as the retrieval methods from ground. Afterwards we describe the instruments and data processing tools used within this study in Sect. 3. In Sect. 4 cloud adiabacity is investigated. Subsequently we contrast important key properties for aerosol-cloud interactions from SEVIRI and LACROS and discuss uncertainties from both perspectives (Sect. 5). Finally, a conclusion and outlook is given in Sect. 6.

2   Cloud retrieval methods using the sub-adiabatic cloud model

In this section we present the theory of the sub-adiabatic cloud model and retrieval strategies for ground-based instruments as well as passive satellite observations.

For a moist rising air parcel we assume that the liquid water content $q_L(z)$ increases linearly with height (Albrecht et al., 1990):

$$q_L(z) = f_{ad}\Gamma_{ad}(T,p)z \qquad (1)$$

$\Gamma_{ad}(T,p)$ is the adiabatic rate of increase of liquid water content. The adiabatic factor f_{ad} can be understood as a reduction of liquid water due to evaporation triggered by the entrainment of drier air masses, which leads to $f_{ad} < 1$ (sub-adiabatic).

Integrating the liquid water content with height yields the liquid water path. Aerosol-cloud interactions are usually studied as changes in cloud properties and radiative effects for a constant liquid water path (Twomey, 1974; Feingold et al., 2003). Therefore we will express all following physical quantities as function of given liquid water path. Observing the cloud geometrical depth in combination with the liquid water path, and knowing $\Gamma_{ad}(T,p)$, the adiabatic factor can be calculated:

$$f_{ad}(Q_L, H) = \frac{2Q_L}{H^2\Gamma_{ad}(T,p)} \qquad (2)$$

The geometrical depth for adiabatic clouds is obtained by resorting this equation:

$$H(Q_L, f_{ad}) = \sqrt{\frac{2Q_L}{f_{ad}\Gamma_{ad}}} \qquad (3)$$

The equivalent mean volume droplet radius in a cloud depends on the cloud droplet number concentration N_d and the liquid water content:

$$r_V = \sqrt[3]{\frac{3q_L}{4\pi\rho_w N_d}} \qquad (4)$$

In the following we assume homogeneous mixing and introduce the effective radius. The effective radius is defined as the third over the second moment of the droplet size distribution (Hansen and Travis, 1974) and is typically retrieved in remote sensing. The effective radius is related to the mean volume radius introducing a factor k_2 that depends on the width of the droplet size distribution.

$$r_e = k_2^{-\frac{1}{3}} r_V \qquad (5)$$

Typical values for k_2 are 0.67 and 0.8 for marine and continental clouds (Brenguier et al., 2000), respectively. More details on the factor k_2 for the assumed gamma-size distribution can be found in the Appendix.

By substituting r_V with r_e in eq. 4, we yield the effective radius representative for the uppermost cloud layer:

$$r_e(Q_L, f_{\mathrm{ad}}, N_d) = \frac{\sqrt[6]{18 f_{\mathrm{ad}} \Gamma_{\mathrm{ad}} Q_L}}{\sqrt[3]{4\pi\rho_w k_2 N_d}} \qquad (6)$$

To study the microphysical response of aerosols on cloud microphysics with remote sensing techniques, together with the effective radius the optical depth is often used since both can be easily derived from e.g. passive satellite observations (Nakajima and King (1990)).

The optical depth in the sub-adiabatic model can be expressed as a function of Q_L and r_e (Wood, 2006):

$$\tau = \frac{9Q_L}{5\rho_w r_e} \qquad (7)$$

Using this equation the liquid water path can be derived from passive satellite observations.

By substituting r_e from eq. 6, we yield τ as a function of Q_L, N_d and f_{ad}:

$$\tau(Q_L, f_{\mathrm{ad}}, N_d) = \frac{9 \sqrt[3]{4\pi k_2 N_d} \sqrt[6]{Q_L^5}}{5 \sqrt[6]{18\rho_w^4 f_{\mathrm{ad}} \Gamma_{\mathrm{ad}}}} \qquad (8)$$

From this equation, the cloud droplet number concentration from passive satellite observations can be calculated:

$$N_d(Q_L, f_{\mathrm{ad}}, \tau) = \frac{20\rho_w^2 \tau^3 \sqrt{10 f_{ad} \Gamma_{ad}}}{9\pi k_2 \sqrt{Q_L^5}} \qquad (9)$$

To retrieve τ and r_e from the given ground-based observations, the cloud droplet number concentration N_d is substituted in eq. 6 applying a radar-radiometer retrieval approach (e.g. Fox and Illingworth, 1997; Rémillard et al., 2013, see appendix):

$$N_d(Q_L, Z) = \frac{9k_6 Q_L^2}{2\pi^2 \rho_w^2 \left(\int_{CBH}^{CTH} \sqrt{Z(z)} dz\right)^2} \qquad (10)$$

Then we find the optical depth and effective radius for given liquid water path to depend on the width of the droplet size distribution (k_2, k_6), the sub-adiabatic factor (f_{ad}) and the integrated radar reflectivity profile ($\int Z(z)dz$). It follows that $\tau \propto (k_2 k_6)^{\frac{1}{3}}$ and $r_e \propto (k_2 k_6)^{-\frac{1}{3}}$ (Brandau et al., 2010).

While in this study homogeneous mixing is assumed, in general two extremes of mixing processes can be considered (Baker et al., 1982; Boers et al., 2006): (a) homogeneous mixing, where $N_d(z)$ stays constant in the vertical layer, but the droplet radius ($r_V(z)$) is changed due to evaporation, (b) inhomogeneous mixing, where the number of droplets change (dilution of whole droplets), but the droplet radius profile is unchanged. In nature, a mixture of both processes may likely occur (Lehmann et al., 2009). Without entrainment, we find $f_{\mathrm{ad}} = 1$ (adiabatic clouds). The assumption of homogeneous mixing is supported by observations from Pawlowska et al. (e.g. 2000, 2006). The adiabatic factor in this study is considered as representative for the full vertical cloud depth. For such an adiabatic factor f_{ad} a range of $[0.3, 0.9]$ is seen as common (Boers et al., 2006).

Different values for k_2, Γ_{ad} and f_{ad} in eq. 9 have been considered in previous studies using passive satellites (Table 1) due to various reasons (e.g. different cloud regimes, continental vs. maritime). Often even adiabatic clouds are assumed ($f_{\mathrm{ad}} = 1$) in the retrieval process (e.g. Quaas et al., 2006).

3   Data

3.1   Instruments and retrievals

Satellite data from SEVIRI (Schmetz et al., 2002) is used, which provides 12 spectral channels covering the visible, the near infrared, and the infrared spectrum. The channels used here have a nadir resolution of 3 km x 3 km, which decreases towards the poles and is about 4 km x 6 km over our region of interest (Central Europe). In this study we use the 5-min temporal resolution data from the Rapid Scan Service (RSS). The SEVIRI radiances in the different channels are used as input for the Nowcasting Satellite Application Facility (NWC SAF) algorithm (Derrien, 2012) which provides a cloud mask, cloud top height, and cloud classification. To obtain the cloud mask, different multispectral tests using SEVIRI channels are applied in order to discriminate

cloudy from cloud-free pixels. The cloud top height for low, liquid clouds is obtained by using a best fit between measured brightness temperatures in the 10.8 μm channel and simulated values using the RTTOV radiative transfer model (Saunders et al., 1999) applied to atmospheric profiles from the ECMWF (European Centre for Medium-Range Weather Forecasts) numerical weather prediction (NWP) model.

The NWC SAF cloud mask is used in order to derive cloud phase, cloud optical depth, and effective radius with the KNMI (Royal Netherlands Meteorological Institute) cloud physical properties (CPP) algorithm (Roebeling et al., 2006), developed in the context of the satellite application facility on climate monitoring (CM SAF, Schulz et al., 2009). Using a channel in the visible spectrum (0.6 μm) together with an absorbing channel in the near infrared (1.6 μm) (Nakajima and King, 1990), the CPP algorithm retrieves cloud optical depth as well as the effective radius representative for the uppermost cloud part. As this method relies on solar reflectance channels, it is applied only during daytime.

Also data from MODIS is used within this study. MODIS is an imaging spectrometer onboard the satellites Terra (descending node) and Aqua (ascending node) which probe the Earth's atmosphere from a polar orbit that results in one daytime overpass per satellite per day over the region of interest. MODIS measures in 36 bands in the visible, near-infrared, and infrared spectrum, with some bands having a spatial resolution of up to 250 m. The cloud physical properties (Platnick et al., 2003) are retrieved in a similar manner as for SEVIRI, but at 1 km spatial resolution using the channels 0.6 μm (band 1, over land) and 2.1 μm (band 7, over land and sea). In addition, effective radius retrievals are available using the channels at 1.6 μm (band 6) and 3.7 μm (band 20) together with band 1. Note that band 6 on the Aqua satellite suffers from a stripe-problem (Wang et al., 2006). In this study MODIS collection 6 is used for the retrieved cloud optical depth and effective radius.

The ground-based remote sensing instruments of the Leipzig Aerosol and Cloud Remote Observations System (LACROS) comprise a 35-GHz MIRA-35 cloud radar, a HATPRO (Humidity And Temperature PROfiler) microwave radiometer, and a CHM15X ceilometer, which are used also for field campaigns. All instruments are operated in a vertically pointing mode. The raw measurements are processed with the Cloudnet algorithm package (Illingworth et al., 2007). The output data is available in an unified temporal resolution of 30 s and a vertical grid of 30 m. Cloudnet uses further information from a NWP model (here: COSMO-DE). In this study we use the attenuation-corrected radar reflectivity from the cloud radar, the liquid water path obtained from the microwave radiometer, as well as the cloud base and top height retrieved from ceilometer and cloud radar, respectively. The vertical Doppler velocity from the cloud radar is also utilized. Furthermore Cloudnet provides a target classification applying a series of tests to discriminate cloud phase, drizzle or rain, and aerosols or insects.

3.2 Data selection

For this study, we use a 2 year period covering 2012 and 2013. We focus on ideal cases to gain a better understanding of the microphysical processes within the cloud. In order to avoid uncertainties caused by inhomogeneous cloud scenes, such as multi-layer clouds, we consider single-layer cloud systems which are entirely liquid and non-drizzling as ideal.

Cloud profiles as observed from the ground are filtered according to the following conditions:

– No occurence of drizzle/rain in Cloudnets target classification (and no drizzle/rain in the 2 nearest neighbour profiles allowed.)

– Values of LWP are between 25 gm^{-2} and 400 gm^{-2}. The lower limit is due to typical instrument uncertainty of the microwave radiometer and the upper limit due to typical thresholds for drizzle occurence (Löhnert et al., 2001).

– The liquid cloud layer must be situated between 300 m and 4000 m above ground.

– The cloud geometrical depth is between 100 m and 2000 m.

– No ice cloud layer within the first 4000 m above ground is present. Thin ice cloud layers above are excluded from calculation of cloud geometrical depth. The microwave radiometer is not sensitive to ice, so that the LWP should not be affected.

– No vertical gaps in the cloud layer are present.

– Z_{max} < -20 dBZ within the cloud profile to avoid occurence of drizzle (Rémillard et al., 2013; Mace and Sassen, 2000).

The comparison of optical and microphysical properties between ground-based and MODIS and SEVIRI is only applicable under daytime conditions. Thereby, we have to consider the different spatial and temporal resolution, as well as the different viewing zenith angle on the cloudy scene. For SEVIRI a parallax shift occurs at higher latitudes. The satellite viewing zenith angle for Leipzig is 58.8 °. Within this study the average cloud top height is between 1 km and 3 km (see Table 2). This would result in a horizontal displacement of max. 5 km. Greuell and Roebeling (2009) did find a significant difference only for inhomogeneous clouds considering parallax correction. Taking also into account the spatial resolution of SEVIRI over Central Europe of 4 km x 6 km, we decided to neglect the parallax correction for our study, instead we consider surrounding pixels. For SEVIRI a field of 3x3 pixels (case studies), and 5x5 pixels (longer-term statistics) centered on the ground site is used and spatially averaged.

We will furthermore present four hand-selected cases to highlight specific problems more closely. For the four case

days, we calculate the spatial inhomogeneity parameter following Cahalan et al. (1994), using the 3x3 SEVIRI pixel field, which can be interpreted also in terms of temporal inhomogeneity (χ) if advection of clouds over a fixed location is considered:

$$\chi = \frac{\exp{(\overline{\ln \tau})}}{\overline{\tau}} \qquad (11)$$

A short overview of the case characteristics is given in table 2. The cloud boundaries are shown along with the cloud radar reflectivity profile in Fig. 1. The synoptic conditions for the cases are as follows. A high pressure system dominates the synoptic weather pattern on 21 October 2011 (Fig. 1a). The temperature at the 850 hPa pressure level over Leipzig is around 5 °C. Therefore the stratocumulus cloud layer that is observed between 10:30Z and 13:00Z consists entirely of water droplets. Its geometrical depth increases in the beginning of the observation period. The weather pattern on 21 April 2013 (Fig. 1b) is quite similar with the high pressure influence being stronger. The temperatures at the 850 hPa pressure level are slightly positive. During the whole observation period at Krauthausen a closed cloud deck is visible. The ground-obtained cloud top height shows only small variability, while the cloud base is more inhomogeneous during the beginning of the observation period. A thin overlying Cirrus cloud deck can be observed around 10:00Z and between 11:00Z - 12:00Z. An upper-level ridge covers Central Europe on 1 June 2012 (Fig. 1c), but the area around Leipzig is also influenced by a surface low. Temperatures at 850 hPa lie around 10 °C. The stratocumulus cloud deck with the cloud tops slightly below 2000 m between 12:00Z and 14:00Z is broken. The weather pattern for the 27 September 2012 (Fig. 1d) shows Leipzig directly in front of a well pronounced trough. Temperatures at 850 hPa lie again around 10 °C and the cloud types vary between stratocumulus and shallow cumulus. The cloud base height increases throughout the day.

4 Cloud adiabacity

Entrainment of dry air into the clouds leads to evaporation of cloud water and therefore to a deviation from the adiabatic liquid water content profile. Knowledge of the adiabatic factor is required to calculate key quantities for investigating aerosol-cloud-interactions from passive satellite observations. Therefore we first study cloud adiabacity, before conducting a intercomparison of ground-based and satellite key properties as well as discuss sources of its uncertainties. The adiabatic factor can be calculated from the ground-based observations. We will further investigate possibilities to estimate it from passive satellite observations.

4.1 Adiabatic factor from ground-based observations

The ground-based adiabatic factor (f_{ad}) is calculated using Q_{L} from the microwave radiometer, H as the difference of cloud top height from the cloud radar and cloud base height from the ceilometer, and $\Gamma_{\text{ad}}(T_{\text{cbh}}, p_{\text{cbh}})$ using NWP data in Eq. (2).

Boers et al. (2006) suggests a range of typical values of $[0.3, 0.9]$. We omitted adiabatic factors with $f_{\text{ad}} > 1.0$ since those are most likely affected by the measurement uncertainties, since the occurence of "superadiabatic" cloud profiles in nature is physically implausible. Such artefacts especially arise due to uncertainties in Q_{L} and H for thin clouds. In contrast to the original Cloudnet code, our calculation of the adiabatic factor allows for $f_{\text{ad}} > 1.0$. Within Cloudnet "superadiabatic" profiles are avoided by increasing the cloud top height if the integrated adiabatic q_{L} is smaller than Q_{L} measured by the microwave radiometer.

An example time-series for one case (21 April 2013) is shown in Fig. 2 (see the supplements for more cases). For this we find values of the adiabatic factor f_{ad} between 0.2 and 0.6 before 09:00 UTC. The radar reflectivity measurements (Fig. 1b) reveal that the cloud base is more inhomogeneous during this time period than later on. After 09:00 UTC the adiabatic factor varies between 0.5 and 1.0.

From Fig. 3a we find a mean of $f_{\text{ad}} = 0.63$ and the IQR as $[0.46, 0.81]$ for the entire dataset covering 2012 and 2013. This corresponds well with the typical value of 0.6 given by Boers et al. (2006). Overall, there is a large spread of values covering the full physical meaningful range from 0 to 1 (mean values for individual cases as presented in Fig. 1 are listed in Table 4). The adiabatic factor is not only changing from case to case, but also varying with time for individual days, reflecting the natural variability of entrainment processes. The variability of the adiabatic factor is larger for the inhomogeneous cases than for the homogeneous ones (Table 4), but the range of values is similar. This shows that independent from temporal cloud homogeneity the majority of clouds seems to be sub-adiabatic. Therefore considering a constant adiabatic factor like in previous studies (Table 1) is problematic.

When looking for proxies for the adiabatic factor, we find a tendency that geometrically thicker clouds are less adiabatic (Figure 3b). Already Warner (1955) found a decrease in the adiabatic factor with height. It also supports the findings of Min et al. (2012), who observed the tendency that thicker clouds are less adiabatic in the Southeast Pacific. Mainly the thin clouds ($H < 400$ m) result in $f_{\text{ad}} > 1$, as also found by Miller et al. (1998), and therefore the investigation of such thin clouds remains challenging.

Schmidt et al. (2014) used observations of two cases with temporally homogeneous stratocumulus clouds over Leipzig, Germany, and found that in case of updrafts in clouds, the q_{L} profile tends to be more adiabatic. To investigate if such a behaviour also occurs for our cases we apply the cloud

radar Doppler velocity at the cloud base. The average vertical velocity at cloud base for all samples in 2012 and 2013 is found to be -0.1 ms^{-1} with the majority of points (93%) in the range [-1,1] ms^{-1}. Considering the vertical velocity as function of cloud adiabacity (Fig 3c) we find a large spread, which makes it difficult to detect a distinct influence of updraft speed on cloud adiabacity. However, the notch around the median in the box-whisker-plot does not overlap for updraft and downdraft regimes. According to Krzywinski and Altman (2014) the median can be judged to differ significantly on the 95% confidence interval if there is no overlay in the notches. We further calculate the median adiabatic factor for updraft and downdraft regimes for the four selected cases, and find for three out of four cases that clouds are slightly more adiabatic in the updraft regime (Table 4). This behaviour is expected from adiabaticity and also supported by the findings of Schmidt et al. (2014). They report that this effect is strongest at the cloud base and blurs when the data points are averaged over the whole cloud profile.

4.2 Adiabatic factor from satellite observations

From ground-based observations we can show that the adiabatic factor is highly variable even for one location. Therefore we can also expect strong variability for cloud regimes over different regions observed by satellite (e.g. maritime vs. continental). To obtain ACI key quantities from passive satellite observations the adiabatic factor is required over a larger domain. The DWD operates a ceilometer network in Germany (Flentje et al., 2010) which can be used to obtain the cloud base height (CBH). The question remains if Q_L and CTH from SEVIRI are accurate enough to allow for an estimate of the adiabatic factor using Eq. 2. To adress this question, we contrast Q_L and CTH obtained from SEVIRI with LACROS.

We investigate liquid clouds in a two-year period covering 2012 and 2013. Since the estimate of the adiabatic factor from passive satellite observations is expected to be applied over a larger domain, it should be independent from ground-based information. Therefore the sampling is now done in terms of satellite observed quantities. An area of 5x5 pixels (total of 25 pixels) centered at the location of LACROS is considered for each available SEVIRI observation. For this pixel field we obtain average, standard deviation of CTH and the liquid cloud fraction. The liquid fraction is determined by the cloud type classification for each pixel from CPP. We require 90% of the pixel field (23 out of 25 pixels) to be classified as pure liquid clouds. As additional constraint, the standard deviation of CTH for the 25 pixels has to be smaller than 400 m. For LACROS we use the observation averaged using a window of 10 minutes around the SEVIRI observation time. No requirements regarding the cloud phase are made for LACROS.

We first look at the CTH, which can be compared at day- and nighttime. The ground-based instruments give the actual geometrical CTH while from passive satellites a radiative CTH is obtained. Ignoring this physical difference we can see that the SEVIRI CTH is positively biased (Fig. 4a). Derrien et al. (2005) reports a very similar overestimation (320 m) with a large standard deviation of 1030 m for low, opaque clouds. Considering the central pixel of the field does not change the result significantly, showing that the cloud fields are rather homogeneous and should therefore be suitable for such a comparison. The observed bias is not explained by the limited vertical step size of 200 m in the SEVIRI CTH product. A likely explanation of this bias is found in the representation of inversions. Splitting the sample by model inversions did not provide significantly better results, but the actual inversions might not be well represented by the model. Such a case can be seen for 27 October 2011. There, the CTH is roughly 1000 m lower than for the other 3 cases presented here, but the retrieved satellite CTH lies at 2000 m. Considering the closest radiosounding of Lindenberg (Germany), we find two inversion layers on top of each other between 900 m and 3000 m, which results in ambiguities in finding the correct cloud height. Differences may also result from semitransparent cirrus cloud layers (21 April 2013), or broken cloud conditions (1 June 2012 and 27 September 2012).

For the comparison of Q_L we impose the condition that the values are between 20 gm^{-2} and 400 gm^{-2}. The comparison can only be applied during daytime. Both requirements reduce the number of samples by 56% compared to the CTH sample. The difference of Q_L has a distribution with a distinct peak close to zero (Fig. 4c). There is a small negative bias of -21 gm^{-2}, which is within the uncertainty range of the ground-based measurements, not even considering the uncertainty of the satellite-based estimate. Similar to the CTH comparison we see that the distribution of the central pixel is not significantly different from the field average, although the spread is larger. The distribution and the standard deviation are consistent with the observations in the validation study of Roebeling et al. (2008b) for the Cloudnet stations of Chilbolton and Palaiseau. Similar to their study we see a slight negative skewness, which stems from larger Q_L values seen from the ground-based MWR. Roebeling et al. (2008b) also reported that accuracy is reduced for higher Q_L values. Further possible explanations for differences in Q_L observed from ground and SEVIRI can be found in remaining cloud inhomogeneities and sampling differences. Generally, unfavorable viewing angles that occur especially in winter conditions can lead to large uncertainties in the satellite retrieval. In our sample the majority of the cases occur in summer months (April to September, 80%). Looking at specific case days, we find the mean difference of Q_L for two homogeneous cases between SEVIRI and the ground-based MWR in reasonable agreement (8 gm^{-2} (10%) for 21 April 2013, 25 gm^{-2} (32%) for 27 October 2011), while there are larger differences for two inhomogeneous cases (50 gm^{-2} (87%) for 1 June 2012 and 33 gm^{-2} (80%) for 27 September 2012).

A similar study by Meerkötter and Zinner (2007) found a standard deviation of 369 m between satellite-based adiabatic CBH and ceilometer CBH. They applied CTH and Q_L from AVHRR (Advanced Very High Resolution Radiometer) and assumed adiabatic clouds to compare the spatially and temporally averaged satellite product. The same comparison between SEVIRI and radiosonde observations resulted in a standard deviation of ± 290 m (Meerkötter and Bugliaro, 2009). They suggest that this method can be applied for convective clouds in their early growth stage, which are located near the condensation level. Their sample is focused on relatively thin water clouds (~250 m), which are more likely close to adiabacity according to our Fig. 3b. As we will discuss in the following the adiabatic factor for such thin clouds is very sensitive to errors in cloud geometrical depth, so that an instantaneous retrieval of the adiabatic factor is not feasible.

4.3 Uncertainty estimate of the adiabatic factor

To investigate the uncertainties that influence the calculation of the adiabatic factor, we consider an adiabatic cloud ($f_{ad} = 1$) with $Q_L = 100\,\mathrm{gm}^{-2}$ and $H = 324$ m and $\Gamma_{ad} = 1.9 \cdot 10^{-3}\,gm^{-4}$. The Q_L retrieval uncertainty (microwave radiometer instrument error + retrieval error) is approximately $25\,\mathrm{gm}^{-2}$ and the vertical resolution of the ceilometer and the cloud radar results in at least ± 60 m uncertainty of H. Accounting for the maximum uncertainty ($Q_L = 125\,\mathrm{gm}^{-2}$, and $H_{obs}^{ground} = 264$ m) or ($Q_L = 75\,\mathrm{gm}^{-2}$ and $H_{obs}^{ground} = 384$ m), the resulting adiabatic factor would be 1.89 or 0.54, respectively. This shows that with the current uncertainty limits of the ground-based observations the adiabatic factor is still prone to large uncertainties especially for geometrically thin clouds.

If we consider the root mean square differences (RMSD) of the comparison of ground and satellite-based values with $\Delta Q_L = 67\,\mathrm{gm}^{-2}$ and $\Delta \mathrm{CTH} = 1174$ m, we can clearly see that especially the observed bias in CTH can result in large uncertainties of an instantaneous estimate of the adiabatic factor especially for thin clouds. For the adiabatic cloud considered above, this RMSDs result in a relative uncertainty for the adiabatic factor of 727%, neglecting uncertainties at the CBH. Even considering a cloud that is twice thick, the relative uncertainty is still 362%. This shows that subsampling the SEVIRI observations to homogeneous, liquid clouds does still show differences when compared to a ground-based reference that are too large to estimate the adiabatic factor with sufficient reliability, mainly due to uncertainties in the CTH product. With this approach using Q_L and H we cannot determine the adiabacity of clouds with a reasonable accuracy. Therefore we will have a look on the microphysical quantities.

5 Microphysical key quantities for aerosol-cloud interactions

The cloud geometrical depth H and cloud droplet number concentration N_d are used as the main parameters in many investigations of aerosol cloud interactions (and therefore the first indirect aerosol effect) as both cloud properties have a direct effect on cloud albedo. Due to the required assumptions about the droplet size distribution a retrieval of cloud droplet number concentration from a radar-radiometer approach remains highly uncertain. Brandau et al. (2010) follows an alternative approach to retrieve τ instead of N_d and demonstrated it to be less sensitive to the assumption of the width of the droplet size distribution.

In the following, we will cross-check key quantities H and τ from ground and satellite. We will also discuss the effect of uncertainties in our observations for the sub-adiabatic cloud model on N_d, τ and H.

5.1 Cloud geometrical depth H intercomparison from space and ground

Contrasting SEVIRI H (eq. 3, using f_{ad} from ground-based observations) with the LACROS H, we are able to investigate the same quantity obtained with two independent physical retrieval approaches.

The correlation coefficient is 0.89 for 21 April 2013, 0.70 for 27 October 2011, 0.38 for 1 June 2012, and 0.45 for 27 September 2012 and increases by 10%, 39%, 118% and 71% for 30 min temporal averaging, respectively (see Table 5). The improvement of correlation is not surprising when comparing averaged data (e.g. Deneke et al., 2009; McComiskey and Feingold, 2012). However, a longer averaging period removes the original variability of the data. The correlation for temporally averaged data is within the range of values that were obtained by Roebeling et al. (2008b), Min et al. (2012) and Painemal and Zuidema (2010). Roebeling et al. (2008b) found correlations of 0.71 between SEVIRI and Cloudnet for a homogeneous stratocumulus cloud layer. Min et al. (2012) found correlations of 0.62 between in-situ and MODIS retrieved H, and could show a better agreement of H when the adiabatic factor is explicitly calculated and considered. Painemal and Zuidema (2010) found correlations of 0.54 (0.7 for $H < 400$ m with cloud fraction$> 90\%$) comparing radiosonde-derived cloud geometrical depth to respective MODIS observations. In their study Painemal and Zuidema (2010) reported that satellite values were higher compared to the ground-based ones. The reason for this can potentially be explained by a bias of MODIS-retrieved r_e but also in the choice of the adiabatic factor in the retrieval of H.

5.2 Cloud optical depth τ intercomparison from space and ground

The intercomparison of SEVIRI with LACROS retrieved τ results in differences of 2.3 (8%) for 21 April 2013, 3.6 (21%) for 27 October 2011, 9.3 (76%) for 1 June 2012 and 8.0 (61%) for 27 September 2012. The higher resolution of the ground-based observations leads to larger variability also for the homogeneous cases. The median conditions result in a good fit to the satellite (τ,Q_L)-pairs (Fig. 5) for the homogeneous case on 21 April 2013. For this case the satellite pairs are also within the ground-based temporal interquartile range (IQR). The situation is similar even for the inhomogeneous case on 1 June 2012. The situation turns out to be more complicated when looking at the inhomogeneous case on 27 September 2012. Overall satellite τ and Q_L show lower values, which result likely due to broken-cloud effects in the SEVIRI retrieval. For broken clouds within the SEVIRI pixel the satellite receives a combined signal from the clouds but also from the surface. Such moving, broken cloud fields result in a smoother temporal pattern from the satellite perspective. From the time-height radar reflectivity cross-section on 27 September 2012 between 11:00 UTC and 15:00 UTC a larger number of cloud gaps can be seen, which could explain why the subpixel surface contamination plays a larger role than on 1 June 2012. The Cloudnet observations on 27 September 2012 show rapid changes of Q_L with peaks around $400 \, gm^{-2}$ and cloud free periods. The observed larger deviations of SEVIRI found on 27 October 2011 are likely due to low values ($<5 \, \mu$m) of effective radius in the KNMI-CPP retrieval. These are likely a result of the unfavourable viewing conditions with a large solar zenith angle ($> 60°$) under relative azimuth angles close to $180°$ around noon for this case, for which Roebeling et al. (2006) pointed out the low precision of the retrieval. These values are filtered out following Roebeling et al. (2008a), but the remaining points might likely also be affected by the same issue.

To highlight the importance of considering the actual adiabatic factor for the retrieval process, we calculated the optical depth (Eq. 7) from the ground-based observations following the radar-radiometer approach with an adiabatic factor $f_{ad} = 1$ and with the ground-obtained adiabatic factor. Afterwards we compare it to the satellite-retrieved values. Applying $f_{ad} = 1$ the mean difference in optical depth is increased from 2.3 to 8.5 on 21 April 2013, and is also higher for the other cases (see Table 6).

The distribution of differences between SEVIRI and ground-based τ for the 2012 and 2013 sample of low-level, homogeneous, liquid clouds is presented in Fig. 4b. As for Q_L there is a distinct peak around zero with negligable bias, but a considerable standard deviation of 16. This shows that on average the agreement between satellite and ground-based τ is reasonable, considering the number of uncertainties in the retrieval as well as uncertainties due to parallax, colloca-tion and spatial resolution. Those uncertainties will be discussed in more detail in the following sections.

5.3 Ground-based uncertainties

The radar-radiometer retrieval depends upon the observations of Q_L, H and $Z(z)$. Also the choice of the mixing model is able to change the retrieved quantities, but Boers et al. (2006) comes to the conclusion that this effect is small. N_d depends further on k_6, which only depends on the width of the droplet size distribution (see Eq. 10 in the Appendix).

We take two typical cloud profiles from our observations. For those cloud profiles we evaluate the sensitivity of the retrieved N_d to the uncertainties of the input parameters based on Brandau et al. (2010). In Table 3 we list the sensitivities to each input parameter when the other parameters are kept constant.

For $Z(z)$ we follow Brandau et al. (2010) and assume an uncertainty range of ± 2 dBZ, which would represent a calibration bias constant with height. Löhnert et al. (2003) points out the strong influence of drizzle on the cloud reflectivity. Errors of 30-60 % have to be anticipated for q_L profile retrievals. Those retrieval approaches are based on very similar principles as the radar-radiometer retrieval method (Löhnert et al., 2001). In our study we filtered out drizzling profiles as well as possible. For the four case days the effective radius observed from satellite near cloud top lies clearly below the value of $14 \, \mu$m which was suggested by Rosenfeld et al. (2012) as the threshold for drizzle/rain forming clouds. The maximum of the radar reflectivity in each profile also did not exceed -20 dBZ, which is commonly taken as a drizzle threshold (Rémillard et al., 2013; Mace and Sassen, 2000). We cannot totally rule out the possibility that few larger droplets were present, for which the radar reflectivity is very sensitive. For the uncertainty of H, we assume ± 60 m. For Q_L we assume a typical uncertainty of $\pm 25 \, gm^{-2}$ given microwave radiometer observations. The width of the droplet size distribution for continental clouds exhibits a large spread of values in literature as can be seen in Miles et al. (2000). If we consider the maximum range of observations, the effective variance ν of the gamma size distribution could take values between 0.2 up to 0.043 ($k_2 = 0.48$ and $k_2 = 0.87$, respectively). For the standard retrieval we assume $\nu = 0.1$ ($k_2 = 0.72$).

N_d is most sensitive to the assumption about the width of the droplet size distribution, especially to changes in the range of smaller values of the effective variance. This can be understood as $N \propto k_6$ and k_6 is a monotonically decreasing function of the effective variance. For higher values of ν the other uncertainty contributions are equally or even more important. Since the real droplet size distribution is usually unknown, it is difficult to estimate the actual uncertainty when assuming $\nu = 0.1$. From our cases we find that the uncertainty in Q_L might be more important than the uncertainty in

radar reflectivity. Both can result in more than 50% relative uncertainty for the retrieval of N_{d}.

As can be seen from Eq. 7, the optical depth τ is sensitive to the same input parameters as N_{d}, but also depends on f_{ad}. Therein the combined uncertainty of Q_{L} and H is reflected. From Table 3 we find that τ is most sensitive to uncertainties in Q_L, especially for observed low values of Q_L. In contrast to N_{d} it is not as sensitive to the assumption about the width of the droplet size distribution. While for N_{d} the uncertainties in the low-range of ν is above 100%, it is below 20% for τ. Since the natural variability of droplet size distributions is large and difficult to constrain without in-situ observations, τ turns out to be a more stable quantity for contrasting to other observation, as already suggested by Brandau et al. (2010).

In Fig. 5 we present the uncertainty of τ as a function of Q_{L}, based on the median observations from the ground-based time-series. We use a representative average of N_{d} over the whole time-period and investigate the effect of its temporal variability on the retrieved τ. Frisch et al. (2002) used a climatological mean value for N_{d} in order to retrieve r_e and reported an average N_{d} of $212 \pm 107\,cm^{-3}$ at the Southern Great Plains site for continental clouds, which is similar to the median value found for our example cases in Fig. 5. We see that assuming a 50% uncertainty for both, N_{d} and τ, results in an increasing uncertainty of τ with Q_{L}, with the uncertainty due to ΔN_{d} being slightly larger, although Δf_{ad} cannot be neglected.

5.4 Satellite uncertainties

5.4.1 Uncertainties of cloud droplet number concentration and cloud geometrical depth

Since cloud droplet number concentration N_{d} is obtained with the sub-adiabatic model using Eq. 9, it depends on the uncertainties of τ and r_e, but also on f_{ad}, k_2 and Γ_{ad}.

Roebeling et al. (2008a) reported a $150\,cm^{-3}$ error for optically thick clouds ($\tau > 20$) resulting from a 10% error in τ. The absolute error of N_{d} increases with increasing τ assuming a constant error in r_e. N_{d} is also very uncertain for values of $r_e < 8\,\mu$m. Han et al. (1994) found that cases with $r_e < 5\,\mu$m are rare compared to typical value of $10\,\mu$m for liquid clouds. Roebeling et al. (2008a) argue that those should not be considered due to the large uncertainty.

If the individual errors are assumed to be normally distributed, the relative errors of N_{d} and H are given by:

$$
\left(\frac{\Delta N_d}{N_d}\right)^2 =
$$

$$
\left(\frac{\Delta k_2}{k_2}\right)^2 + \left(\frac{\Delta \Gamma_{\mathrm{ad}}}{2\Gamma_{\mathrm{ad}}}\right)^2 + \left(\frac{\Delta f_{\mathrm{ad}}}{2 f_{\mathrm{ad}}}\right)^2 +
$$

$$
\left(\frac{\Delta \tau}{2\tau}\right)^2 + \left(\frac{5 \Delta r_e}{2 r_e}\right)^2 \tag{12}
$$

and

$$
\left(\frac{\Delta H}{H}\right)^2 =
$$

$$
\left(\frac{\Delta \Gamma_{\mathrm{ad}}}{2\Gamma_{\mathrm{ad}}}\right)^2 + \left(\frac{\Delta f_{\mathrm{ad}}}{2 f_{\mathrm{ad}}}\right)^2 + \left(\frac{\Delta \tau}{2\tau}\right)^2 + \left(\frac{\Delta r_e}{2 r_e}\right)^2 \tag{13}
$$

Uncertainties of τ and r_e stem from the assumption of plane-parallel vertical-uniform cloud layers, partially covered cloud pixels (Zinner and Mayer, 2006), 3D effects (Loeb and Coakley, 1998), and large solar zenith angles (Roebeling et al., 2008a). Uncertainties of effective radius further arise from its vertical profile. The use of different channels results in discrepancies in r_e. MODIS uses a channel centered at $2.1\,\mu$m, while SEVIRI uses $1.6\,\mu$m for the standard retrieval. From MODIS, additional effective radius retrievals from channels at $1.6\,\mu$m and $3.7\,\mu$m are available. Theoretically, the 3.7-μm channel should represent the effective radius closer to the cloud top for adiabatic clouds, while the 2.1-μm and 1.6-μm channels receive the main signal from deeper layers within the cloud. Cloud observations do not always show an increase of effective radius from channel $1.6\,\mu$m over $2.1\,\mu$m to $3.7\,\mu$m as is expected for planeparallel, adiabatic clouds (Platnick, 2000; King et al., 2013). In this study we estimate the uncertainties in passive satellite τ and r_e with 10% following Roebeling et al. (2008a) (SEVIRI) and following Platnick and Valero (1995) (MODIS), although uncertainties are probably larger for unfavourable conditions (large solar zenith angles, broken clouds).

For the adiabatic factor we assume a relative error of 35% considering a constant adiabatic factor (0.6) and its variability (0.22) as obtained from two-year LACROS observations. For comparison Janssen et al. (2011) assumed an uncertainty in the adiabatic factor of 0.3. This resulted in a numerically evaluated error of around 26% considering typical values of effective radius and optical depth.

Janssen et al. (2011) estimated the uncertainty of k_2 to be negligible (around 3%) for $N_{\mathrm{d}} < 100\,cm^{-3}$, following Boers et al. (2006). Bennartz (2007) used a variability of $k_2 = 0.8 \pm 0.1$ in a global study, which results in a relative uncertainty of 12.5%. Brenguier et al. (2011) found a similar mean value for 33 cases of stratocumulus and cumulus clouds with a even smaller variability, even slightly lower than the variability in Martin et al. (1994). Therefore 12.5% might be seen as an upper uncertainty limit for k_2.

By considering the whole seasonal variability of cloud base temperature, Janssen et al. (2011) obtained an error of 24% for the adiabatic lapse rate of liquid water mixing ratio ($\Gamma_{\mathrm{ad}}(T, p)$). In our study Γ_{ad} has a smaller contribution to those uncertainties due to the fact that we are using model data to gain more reliable information about cloud base temperature and pressure instead of considering a constant value of Γ_{ad} as in e.g. Quaas et al. (2006). If we compare Γ_{ad} calculated from satellite cloud top temperature and pressure with

the one calculated from cloud base values observed from ground we find an uncertainty of 15% considering the four case days. As we see deviations in the cloud top height, we believe that this uncertainty can be mainly attributed to incorrect satellite estimates of cloud top temperature and pressure.

Janssen et al. (2011) state for satellite retrievals of N_d (and also H_{ad}) that f_{ad} and Γ_{ad} are the most important uncertainty factors. Considering our uncertainty estimates, the largest contribution to the uncertainty of N_d is given by the relative uncertainty of effective radius (25%), followed by f_{ad} (18%), k_2 (12.5%), Γ_{ad} (7.5%) and τ (5%). Considering the error propagation of H, assuming the same errors as for N_d, we find the largest uncertainty due to the adiabatic factor with 17.5%, followed by Γ_{ad} (7.5%) and τ (5%) and r_e (5%).

The importance of r_e for the retrieval of N_d from passive satellite imagers has already been pointed out by previuos studies. Those were mainly based on observations from MODIS (Painemal and Zuidema, 2010, 2011; Ahmad et al., 2013; Zeng et al., 2014) and report a high bias of MODIS r_e, especially for broken clouds (Marshak et al., 2006). Painemal and Zuidema (2010) also state that the choice of the other parameters in the retrieval (namely k_2, Γ_{ad}) is able to compensate for this effect so that still a good agreement between MODIS retrieved and in-situ values could be achieved. As mentioned before, for our study we focused on the intercomparison of τ instead of N_d, since the ground-based retrieval of τ is less sensitive to the required assumptions.

5.4.2　Uncertainties due to spatial resolution

To investigate the effect of spatial resolution, we use collocated MODIS and SEVIRI observations. We use the products of MODIS at 1 km spatial resolution. We reproject all MODIS pixels to the 3x3 SEVIRI pixels so that both instruments cover the same area. We then average the MODIS 1 km resolution data to SEVIRIs spatial resolution (4 km x 6 km). In a further step we average a 3x3 pixel field from SEVIRI and the MODIS pixels at original resolution and calculate their standard deviation. In this way we tried to use MODIS to account for SEVIRIs' subpixel variability, while neglecting deviations due to the differences of both instruments and retrievals. In Fig. 6 the results for (a) the inhomogeneous case at 1 June 2012 and (b) the homogeneous case at 21 April 2013 are shown. For the inhomogeneous case we can clearly see the large spread of MODIS τ values, which is reduced to a similar range as for SEVIRI τ when averaged to the same spatial resolution. The spread of the optical depth is found larger than for the effective radius. For the homogeneous case the spread is smaller. Differences between MODIS and SEVIRI after averaging are in a similar range for both cases. When comparing averaged data, MODIS and SEVIRI show similar results for both cases. However, the differences, especially in terms of r_e can be of the same magnitude than those to ground-retrieved values. There is considerable difference when taking either the closest pixel to the ground-based location or the spatially averaged value, while the closest pixel does not necessarily result in a better agreement with the ground-based value (Fig. 6). Therefore we can conclude that especially for inhomogeneous cases, the sub-pixel variability introduces an important additional uncertainty factor.

6　Summary and Conclusions

In this work, we aimed to evaluate the consistency and limitation of current ground-based and satellite cloud retrieval products that are used to quantify aerosol-cloud interactions. We used a two year dataset with four selected case studies.

Cloud properties have been used previously for diagnosing aerosol-cloud interactions and specifically the Twomey effect from both ground-based supersites (e.g. Feingold et al., 2003) as well as geostationary passive satellite observations (e.g. Bréon et al., 2002). The sub-adiabatic cloud model as a conceptional tool is commonly applied and modified using an adiabatic factor to account for entrainment within the cloud.

Based on cloud geometric depths obtained from the combination of ground-based cloud radar and ceilometer, and liquid water path from a microwave radiometer, we demonstrated that for a two year dataset, neither the assumption of an adiabatic cloud nor the assumption of a temporally constant sub-adiabatic factor is fulfilled (mean adiabatic factor 0.63 ± 0.22).

As the adiabatic factor is required to estimate key quantities for aerosol-cloud-interaction studies, but cannot be obtained from passive satellite observations within a sufficient uncertainty range, an independent method to estimate the adiabatic factor, and thus the influence of mixing, would be highly desirable for global-scale analyses. We were able to support previous findings which reported that thinner clouds are closer to adiabacity (Min et al., 2012) as well are clouds that show upwind motion at the cloud base (Schmidt et al., 2014).

To investigate aerosol-cloud interactions from passive satellites the cloud droplet number concentration is widely used as a key parameter. An intercomparison with ground-retrieved values is complicated as it turns out that its retrieval from a ground-based radar-radiometer approach is very sensitive to assumptions about the width of the droplet size distribution and the radar calibration. Retrieved values of cloud droplet number concentration can change by more than 135% just due to wrong assumptions made for the width of the droplet size distribution. From passive satellite we find the main sensitivity to uncertainties in the effective radius. We conclude that neither the ground-based nor satellite-based cloud retrieved properties used here allow to obtain a robust instantaneous estimate of cloud droplet concentration, which complicates their use for the study of aerosol-cloud interactions.

We demonstrated that cloud optical depth from ground-based radar-radiometer retrievals is less sensitive to the assumptions about the droplet size distribution and is therefore better suited to investigate indirect aerosol effects, consistent with the conclusions of Brandau et al. (2010). It is most sensitive to uncertainties in the liquid water path (changes of up to 50% for an uncertainty of $25\,\mathrm{gm^{-2}}$ are possible).

Given an independent retrieval of cloud optical depth, e.g. from shadowband radiometer retrievals (Min and Duan, 2005), and information such as radar Doppler velocity (Rémillard et al., 2013), should give further options for validation. Applying such additional observations in an optimal estimation scheme might give the opportunity to better constrain the retrieved cloud droplet number concentration. Also the application of cloud radar scanning capabilities together with radiance zenith measurements might improve the retrieval (Fielding et al., 2014). For validation of those cloud droplet number concentration retrievals accompanying in-situ measurements are required.

Instantaneous comparisons of optical depth between space and ground may result in large differences, especially for broken cloud conditions and unfavourable viewing conditions. Applying spatial and temporal averaging and subsampling to rather homogeneous, liquid clouds leads to a reasonable agreement in cloud optical depth for a majority of observations during a two year period at LACROS, especially considering the large number of assumptions and uncertainties.

Besides the the retrieval uncertainties, differences in spatial resolution affect the comparison not only between space and ground observations, but also between space-based instruments of different resolution and viewing angles (i.e. SEVIRI, MODIS). We highlighted, that especially for inhomogeneous cases, sub-pixel variability is an important uncertainty factor, but that averaging does not necessarily result in a better agreement to ground-based observations than taking the closest pixel to the location. To generalize such results more collocated MODIS, SEVIRI and ground-based observations need to be examined.

Given the network of Cloudnet/ACTRIS in Central Europe this offers the opportunity to investigate the climatology of the adiabatic factor and investigate its regional, seasonal or synoptical dependency in further studies.

With the upcoming Meteosat Third Generation (MTG) satellite (Stuhlmann et al., 2005) a higher spatial resolution of cloud products will be available and should therefore mitigate issues due to spatial resolution for the geostationary perspective. Also the sounder capabilities of MTG should give new opportunities, e.g. to overcome problems of cloud geometrical depth retrievals from passive satellites by using additional information from the oxygen A-band following the method as outlined by (e.g. Yang et al., 2013; Fischer et al., 1991). And therefore might give the possibility to obtain the adiabatic factor over a larger domain.

7 Appendix

To obtain the factors k_2 and k_6 in the sub-adiabatic cloud model a gamma size distribution is assumed in the form of (Hansen and Travis, 1974):

$$
\begin{aligned}
\eta(r) &= Ar^\beta \exp -\Lambda r \qquad (14)\\
&= \frac{\eta_0}{\Gamma(\frac{1-2\nu}{\nu})r_e\,\nu^{\frac{1-2\nu}{\nu}}}\left(\frac{r}{r_e}\right)^{\frac{(1-3\nu)}{\nu}}\exp\left(-\frac{r}{r_e\nu}\right)
\end{aligned}
$$

with

$$
\begin{aligned}
\beta &= \frac{1-3\nu}{\nu}\\
\Lambda &= \frac{1}{r_e\nu}\\
A &= \eta_0\frac{\Lambda^{\beta+1}}{\Gamma(\beta+1)}. \qquad (15)
\end{aligned}
$$

Hereby the effective radius r_e, its effective variance ν and the total number density of droplets η_0 is used. The effective radius is defined as the third over the second moment of the droplet size distribution (Hansen and Travis, 1974) and can be linked to the mean volume radius (r_v) with the following relationship:

$$
r_\mathrm{e}^3 = k_2^{-1}r_\mathrm{v}^3 \qquad (16)
$$

From the gamma size distributions its n-th moments can be derived by (Petty and Huang, 2011):

$$
\begin{aligned}
M_{\eta,n} &= A\int r^{n+\beta}\exp(-\Lambda r)dr\\
&= A\frac{\Gamma(\beta+n+1)}{\Lambda^{(\beta+n+1)}}. \qquad (17)
\end{aligned}
$$

The factor k_2 is then only a function of the width of the droplet size distribution:

$$
k_2 = \frac{M_2(\eta)^3}{M_3(\eta)^2} = (1-2\nu)(1-\nu) \qquad (18)
$$

The radar reflectivity as proportional to the sixth moment of the droplet size distribution can be expressed as a function of the cloud droplet number concentration N_d, the liquid water content q_L and factors that depend on the width of the droplet size distribution (k_6) (Fox and Illingworth, 1997):

$$Z = \frac{9}{2\pi^2 \rho_w^2} k_6 \frac{q_L^2}{N_d}. \tag{19}$$

Similar to k_2, the factor k_6 is defined:

$$k_6 = \frac{M_6(\eta)}{M_3(\eta)^2} = \frac{(\nu+1)(2\nu+1)(3\nu+1)}{(1-2\nu)(1-\nu)} \tag{20}$$

Integrating over the cloud geometrical depth, we can solve the equation for the liquid water path:

$$Q_L = \left(\frac{9}{2\pi^2 \rho_w^2}\right)^{-\frac{1}{2}} \int \frac{1}{k_6(\nu(z))} \sqrt{N_d(z)} \sqrt{Z(z)} dz \tag{21}$$

In the homogeneous mixing model $N_d(z)$ and $\nu(z)$ are assumed constant with height. Rémillard et al. (2013) consideres a column-averaged N_d by weighting with the square-root of radar-reflectivity:

$$\int \sqrt{N_d(z)} dz = \frac{\int \sqrt{N_d(z)} \sqrt{Z(z)} dz}{\int \sqrt{Z(z)} dz} = \sqrt{\overline{N_d}} \tag{22}$$

Using the latter relationship, we yield a retrieval method for the column-averaged $\overline{N_d}$:

$$\overline{N_d}(Q_L, Z, k_6) = \frac{9k_6 Q_L^2}{2\pi^2 \rho_w^2 \left(\int \sqrt{Z(z)} dz\right)^2} \tag{23}$$

Eq. 23 can be substituted into eq. 6 and 7 to eliminate N_d and to obtain a ground-based estimate of τ and r_e.

References

Ackerman, A. S., Toon, O. B., Taylor, J. P., Johnson, D. W., Hobbs, P. V., and Ferek, R. J.: Effects of Aerosols on Cloud Albedo: Evaluation of Twomey's Parameterization of Cloud Susceptibility Using Measurements of Ship Tracks, Journal of the Atmospheric Sciences, 57, 2684–2695, doi:10.1175/1520-0469(2000)057<2684:EOAOCA>2.0.CO;2, 2000.

Ahmad, I., Mielonen, T., Grosvenor, D., Portin, H., Arola, A., Mikkonen, S., Kühn, T., Leskinen, A., Juotsensaari, J., Komppula, M., Lehtinen, K., Laaksonen, A., and Romakkaniemi, S.: Long-term measurements of cloud droplet concentrations and aerosol-cloud interactions in continental boundary layer clouds, Tellus B, 65, 2013.

Albrecht, B. A., Fairall, C. W., Thomson, D. W., White, A. B., Snider, J. B., and Schubert, W. H.: Surface-based remote sensing of the observed and the Adiabatic liquid water content of stratocumulus clouds, Geophys. Res. Lett., 17, 89–92, doi:10.1029/GL017i001p00089, 1990.

Baker, M. B., Blyth, A. M., Carruthers, D. J., Choularton, T. W., Fullarton, G., Gay, M. J., Latham, J., Mill, C. S., Smith, M. H., Stromberg, I. M., Caughey, S. J., and Conway, B. J.: Field studies of the effect of entrainment upon the structure of clouds at Great Dun Fell, Quarterly Journal of the Royal Meteorological Society, 108, 899–916, doi:10.1002/qj.49710845810, 1982.

Bennartz, R.: Global assessment of marine boundary layer cloud droplet number concentration from satellite, Journal of Geophysical Research: Atmospheres, 112, n/a–n/a, doi:10.1029/2006JD007547, 2007.

Boers, R., Russchenberg, H., Erkelens, J., Venema, V., van Lammeren, A., Apituley, A., and Jongen, S.: Ground-Based Remote Sensing of Stratocumulus Properties during CLARA, 1996, Journal of Applied Meteorology, 39, 169–181, doi:10.1175/1520-0450(2000)039<0169:GBRSOS>2.0.CO;2, 2000.

Boers, R., Acarreta, J. R., and Gras, J. L.: Satellite monitoring of the first indirect aerosol effect: Retrieval of the droplet concentration of water clouds, Journal of Geophysical Research: Atmospheres, 111, n/a–n/a, doi:10.1029/2005JD006838, 2006.

Boucher, O., Randall, D., Artaxo, P., Bretherton, C., Feingold, G., Forster, P., Kerminen, V., Kondo, Y., Liao, H., Lohmann, U., et al.: Clouds and aerosols, Climate Change, pp. 571–657, 2013.

Brandau, C., Russchenberg, H., and Knap, W.: Evaluation of ground-based remotely sensed liquid water cloud properties using shortwave radiation measurements, Atmospheric Research, 96, 366 – 377, doi:http://dx.doi.org/10.1016/j.atmosres.2010.01.009, 15th International Conference on Clouds and Precipitation {ICCP} 2008, 2010.

Brenguier, J.-L., Pawlowska, H., Schüller, L., Preusker, R., Fischer, J., and Fouquart, Y.: Radiative Properties of Boundary Layer Clouds: Droplet Effective Radius versus Number Concentration, Journal of the Atmospheric Sciences, 57, 803–821, doi:10.1175/1520-0469(2000)057<0803:RPOBLC>2.0.CO;2, 2000.

Brenguier, J.-L., Burnet, F., and Geoffroy, O.: Cloud optical thickness and liquid water path – does the k coefficient vary with droplet concentration?, Atmospheric Chemistry and Physics, 11, 9771–9786, doi:10.5194/acp-11-9771-2011, 2011.

Bréon, F.-M., Tanré, D., and Generoso, S.: Aerosol Effect on Cloud Droplet Size Monitored from Satellite, Science, 295, 834–838, doi:10.1126/science.1066434, 2002.

Cahalan, R. F., Ridgway, W., Wiscombe, W. J., Bell, T. L., and Snider, J. B.: The Albedo of Fractal Stratocumulus Clouds, Journal of the Atmospheric Sciences, 51, 2434–2455, doi:10.1175/1520-0469(1994)051<2434:TAOFSC>2.0.CO;2, 1994.

Christensen, M. W. and Stephens, G. L.: Microphysical and macrophysical responses of marine stratocumulus polluted by underlying ships: Evidence of cloud deepening, Journal of Geophysical Research: Atmospheres, 116, n/a–n/a, doi:10.1029/2010JD014638, d03201, 2011.

Deneke, H., Knap, W., and Simmer, C.: Multiresolution analysis of the temporal variance and correlation of transmittance and

Table 1. Overview of assumptions made for the (sub-)adiabatic cloud model applied to derive N_d and H in literature studies. The table lists the values chosen for Γ_{ad}, f_{ad} (calc. refers to explicitly calculated values from additional data) and k_2. The table is sorted by publication year starting with the oldest one.

study	location	instrument(s)	derived quantities	Γ_{ad} [$\cdot 10^{-3} gm^{-4}$]	f_{ad}	k_2
Szczodrak et al. (2001)	Eastern Pacific + Southern Ocean	AVHRR	N_d	2.0	n.a.	n.a.
Schüller et al. (2005)	North Atlantic (marine)	MODIS	N_d, H	n.a.	n.a.	n.a.
Boers 2006	Southern Ocean (Cape Grim)	MODIS	N_d, H	const.	0.6	0.87
Quaas 2006, 2008	global	MODIS	N_d	1.9	1.0	0.8
Bennartz 2007	global	MODIS	N_d, H	T-dependent	0.8	0.8
Roebeling 2008	Europe (continental)	SEVIRI	N_d, H	Boers 2006	0.75	Boers 2006
George 2010	Southeast Pacific	MODIS	N_d	1.95	n.a.	n.a.
Painemal 2010	Southeast Pacific	MODIS	N_d, H	2.0	1.0	0.8
Janssen 2011	Finnland (continental)	MODIS	N_d, H	1.44	0.6	0.87
Painemal 2011	Southeast Pacific	MODIS	N_d	2.0	1.0	0.8
Min 2012	Southeast Pacific	MODIS	N_d, H	T-dependent	calc.	0.5-1.0
Ahmad 2013	Puijo (continental)	MODIS	N_d	n.a.	1.0	0.67
Painemal 2013	Southeast Pacific	MODIS, aircraft	N_d	T_{cbh}, p_{cbh}	0.9	0.88
Zeng 2014	global	A-Train	N_d, H	T_{cth}, p_{cth}	1.0	0.6438
this study	Germany (continental)	SEVIRI	N_d, H	T_{cbh}, p_{cbh}	calc.	0.72

Table 2. Cases used within this study sorted by date. The minimum cloud base height (CBH) and the maximum cloud top height (CTH) of the liquid cloud layer investigated are presented together with the temporally averaged inhomogeneity parameter (χ) as in Cahalan et al. (1994) calculated from the optical depth of the ± 2 surrounding SEVIRI pixels for each observation time. Furthermore the category for each case is listed.

Date	Time	Location	Min(CBH) [m]	Max(CTH) [m]	χ	category
27 Oct 2011	10:30–13:00 UTC	Leipzig	526 m	1056 m	0.96	homogeneous
1 Jun 2012	12:00–14:00 UTC	Leipzig	1336 m	2085 m	0.85	inhomogeneous
27 Sep 2012	09:00–16:00 UTC	Leipzig	775 m	2553 m	0.87	inhomogeneous
21 Apr 2013	08:00–12:00 UTC	Krauthausen	1485 m	2171 m	0.99	homogeneous

Table 3. Uncertainty estimation for N_d and τ by varying Z, Q_L and the effective variance of the gamma distribution ν. Relative uncertainties are given in brackets. Case 1: 21 April 2013, 11:00 UTC. $Q_L = 69\,gm^{-2}$, $H = 311$ m, $f_{ad} = 0.76$. Retrieved values: $N_d = 456\,cm^{-3}$ applying ν=0.1, $\tau = 18$. Case 2: 1 June 2012, 13:30 UTC. $Q_L = 62\,gm^{-2}$, $H = 342$ m, $f_{ad} = 0.55$, $N_d = 216\,cm^{-3}$, $\tau = 13.6$.

	ΔN_d (case 1)	ΔN_d (case 2)	$\Delta\tau$ (case 1)	$\Delta\tau$ (case 2)
$\Delta Z = -2\,dBZ$	266 (58%)	126 (58%)	3.0 (17%)	2.3 (17%)
$\Delta Z = +2\,dBZ$	168 (37%)	80 (37%)	2.6 (14%)	1.9 (14%)
$\Delta Q_L = -25\,gm^{-2}$	267 (59%)	140 (64%)	4.7 (26%)	6.8 (49%)
$\Delta Q_L = +25\,gm^{-2}$	384 (84%)	209 (96%)	4.1 (22%)	7.8 (57%)
$\nu = 0.200$	614 (135%)	292 (135%)	2.9 (16%)	2.2 (16%)
$\nu = 0.043$	174 (38%)	83 (38%)	1.7 (9%)	1.3 (9%)

Table 4. Median and standard deviation of the adiabatic factor (calculated from Eq. 2) for individual cases. Furthermore the median of the adiabatic factor, classified into updraft ($v \geq 0$) and downdraft ($v < 0$) regimes, as well as the fraction of subadiatic cloud profiles is shown. Adiabatic factors with $f_{ad} > 1.0$ are omitted because those are likely affected by measurement uncertainties.

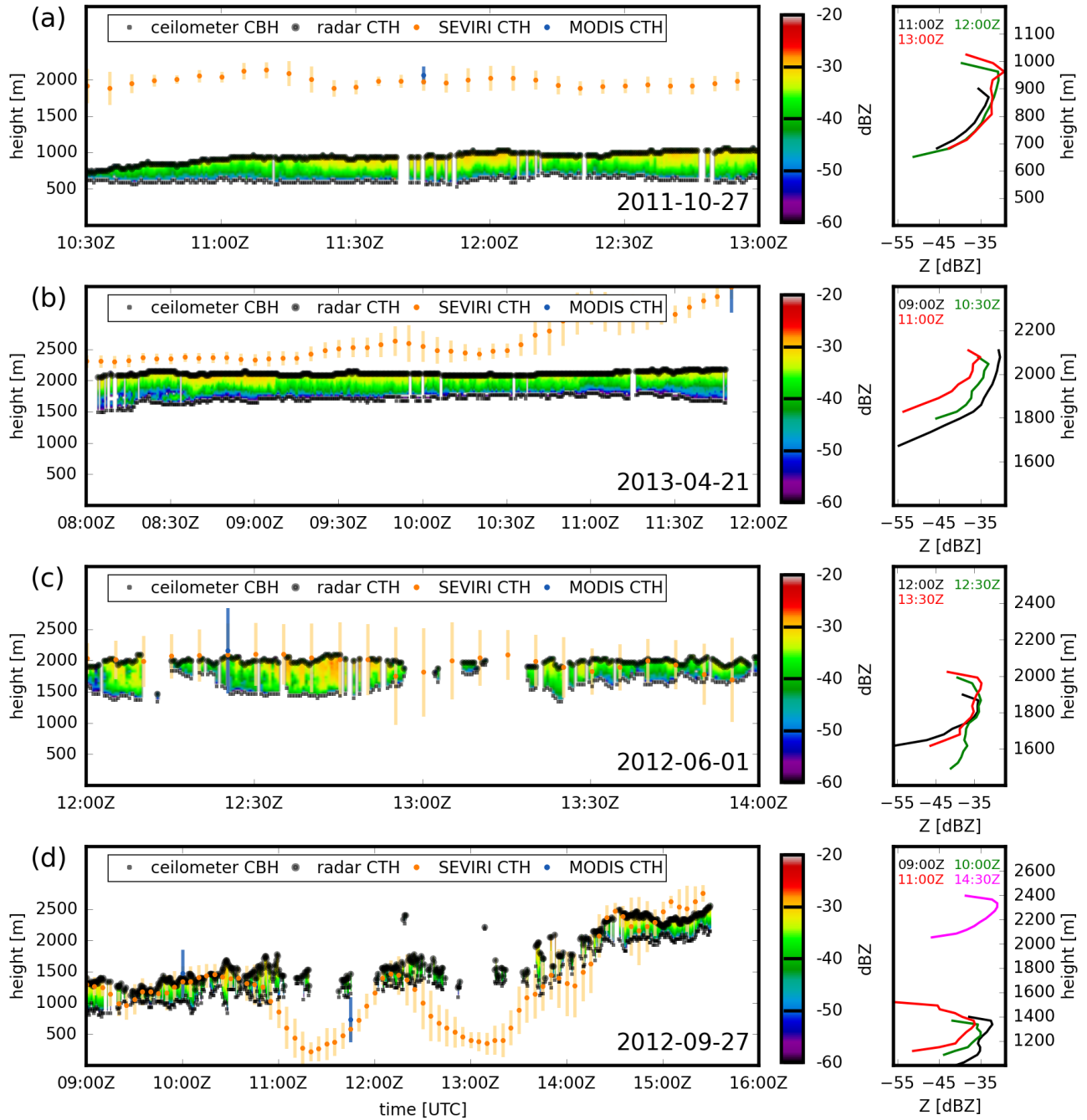|	21 Apr 2013	27 Sep 2012	27 Oct 2011	1 Jun 2012
median f_{ad}	0.63	0.62	0.70	0.44
stddev f_{ad}	0.18	0.21	0.12	0.24
median $f_{ad}\,[v \geq 0]$	0.78	0.64	0.76	0.44
stddev $f_{ad}\,[v \geq 0]$	0.21	0.20	0.12	0.23
median $f_{ad}\,[v \leq 0]$	0.61	0.62	0.66	0.44
stddev $f_{ad}\,[v \leq 0]$	0.17	0.21	0.10	0.24
fraction $f_{ad} < 1$	0.99	0.79	0.99	0.90

Figure 1. Time series of radar reflectivity (in dBZ) and cloud boundaries for the 4 cases listed in Table 2; (a) 27 October 2011, (b) 21 April 2013, (c) 1 June 2012, (d) 27 September 2012. Cloud borders are shown as detected by Cloudnet with black dots and by SEVIRI using NWCSAF in orange dots, and MODIS in blue dots. Sample profiles of radar reflectivity are shown at different times during each case.

reflectance of an atmospheric column, J. Geophys. Res., 114, D17 206, doi:10.1029/2008JD011680, 2009.

Derrien, M.: Algorithm theoretical basis document for cloud products (cma-pge01 v3.2, ct-pge02 v2.2, ctth-pge03 v2.2), Tech. rep., SAFNWC, 2012.

Derrien, M., Gléau, H., Daloze, J.-F., and Haeffelin, M.: Validation of SAFNWC/MSG cloud products with one year of SEVIRI data,

in: 2005 EUMETSAT Meteorological Satellite Conference, pp. 95–103, 2005.

Dong, X., Ackerman, T. P., Clothiaux, E. E., Pilewskie, P., and Han, Y.: Microphysical and radiative properties of boundary layer stratiform clouds deduced from ground-based measurements, Journal of Geophysical Research: Atmospheres, 102, 23 829–23 843, doi:10.1029/97JD02119, 1997.
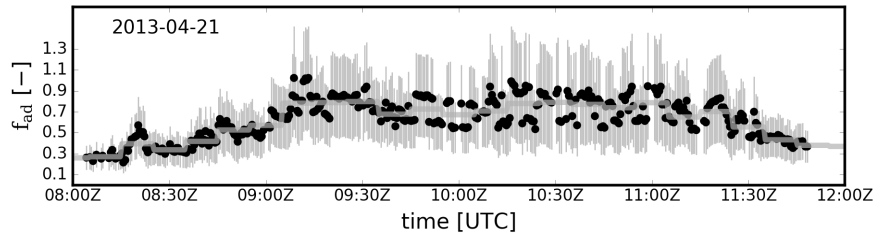
Figure 2. Timeseries of the adiabatic factor for 21 April 2013. Black dots represent the adiabatic factor derived using ground-based geometrical depth and liquid water path from the microwave radiometer. The gray line represents the 10-min averaged and interpolated adiabatic factor neglecting superadiabatic values.

Table 5. Correlation coefficient of cloud geometrical depth from LACROS and from SEVIRI (3x3 pixel spatial average) for different temporal averaging periods applied to both datasets.

Date	5 min average	10 min average	30 min average
21 Apr 2013	0.89	0.96	0.98
27 Oct 2011	0.70	0.72	0.97
27 Sep 2012	0.45	0.61	0.77
01 Jun 2012	0.38	0.53	0.83

Dong, X., Mace, G. G., Minnis, P., Smith, W. L., Poellot, M., Marchand, R. T., and Rapp, A. D.: Comparison of Stratus Cloud Properties Deduced from Surface, GOES, and Aircraft Data during the March 2000 ARM Cloud IOP, Journal of the Atmospheric Sciences, 59, 3265–3284, doi:10.1175/1520-0469(2002)059<3265:COSCPD>2.0.CO;2, 2002.

Feingold, G., Eberhard, W. L., Veron, D. E., and Previdi, M.: First measurements of the Twomey indirect effect using ground-based remote sensors, Geophysical Research Letters, 30, n/a–n/a, doi:10.1029/2002GL016633, 2003.

Fielding, M. D., Chiu, J. C., Hogan, R. J., and Feingold, G.: A novel ensemble method for retrieving properties of warm cloud in 3-D using ground-based scanning radar and zenith radiances, Journal of Geophysical Research: Atmospheres, 119, 10,912–10,930, doi:10.1002/2014JD021742, 2014.

Fischer, J., Cordes, W., Schmitz-Peiffer, A., Renger, W., and Mörl, P.: Detection of Cloud-Top Height from Backscattered Radiances within the Oxygen A Band. Part 2: Measurements, Journal of Applied Meteorology, 30, 1260–1267, doi:10.1175/1520-0450(1991)030<1260:DOCTHF>2.0.CO;2, 1991.

Flentje, H., Heese, B., Reichardt, J., and Thomas, W.: Aerosol profiling using the ceilometer network of the German Meteorological Service, Atmospheric Measurement Techniques Discussions, 3, 3643–3673, doi:10.5194/amtd-3-3643-2010, 2010.

Fox, N. I. and Illingworth, A. J.: The Retrieval of Stratocumulus Cloud Properties by Ground-Based Cloud Radar, Journal of Applied Meteorology, 36, 485–492, doi:10.1175/1520-0450(1997)036<0485:TROSCP>2.0.CO;2, 1997.

Frisch, A. S., Fairall, C. W., and Snider, J. B.: Measurement of Stratus Cloud and Drizzle Parameters in ASTEX with a Ka-Band Doppler Radar and a Microwave Radiometer, Journal of the Atmospheric Sciences, 52, 2788–2799, doi:10.1175/1520-0469(1995)052<2788:MOSCAD>2.0.CO;2, 1995.

Frisch, S., Shupe, M., Djalalova, I., Feingold, G., and Poellot, M.: The Retrieval of Stratus Cloud Droplet Effective Radius with Cloud Radars, Journal of Atmospheric and Oceanic Technology, 19, 835–842, doi:10.1175/1520-0426(2002)019<0835:TROSCD>2.0.CO;2, 2002.

Greuell, W. and Roebeling, R. A.: Toward a Standard Procedure for Validation of Satellite-Derived Cloud Liquid Water Path: A Study with SEVIRI Data, Journal of Applied Meteorology and Climatology, 48, 1575–1590, doi:10.1175/2009JAMC2112.1, 2009.

Han, Q., Rossow, W. B., and Lacis, A. A.: Near-Global Survey of Effective Droplet Radii in Liquid Water Clouds Using ISCCP Data, Journal of Climate, 7, 465–497, doi:10.1175/1520-0442(1994)007<0465:NGSOED>2.0.CO;2, 1994.

Han, Q., Rossow, W. B., Chou, J., and Welch, R. M.: Global variation of column droplet concentration in low-level clouds, Geophysical Research Letters, 25, 1419–1422, doi:10.1029/98GL01095, 1998.

Hansen, J. E. and Travis, L. D.: Light scattering in planetary atmospheres, Space Science Reviews, 16, 527–610, 1974.

Illingworth, A., Hogan, R., O'connor, E., Bouniol, D., Delanoë, J., Pelon, J., Protat, A., Brooks, M., Gaussiat, N., Wilson, D., et al.: Cloudnet: Continuous evaluation of cloud profiles in seven operational models using ground-based observations, Bulletin of the American Meteorological Society, 88, 883–898, 2007.

Janssen, R. H. H., Ganzeveld, L. N., Kabat, P., Kulmala, M., Nieminen, T., and Roebeling, R. A.: Estimating seasonal variations in cloud droplet number concentration over the boreal forest from satellite observations, Atmospheric Chemistry and Physics, 11, 7701–7713, doi:10.5194/acp-11-7701-2011, 2011.

Kim, B.-G., Miller, M. A., Schwartz, S. E., Liu, Y., and Min, Q.: The role of adiabaticity in the aerosol first indirect effect, Journal of Geophysical Research: Atmospheres, 113, n/a–n/a, doi:10.1029/2007JD008961, d05210, 2008.
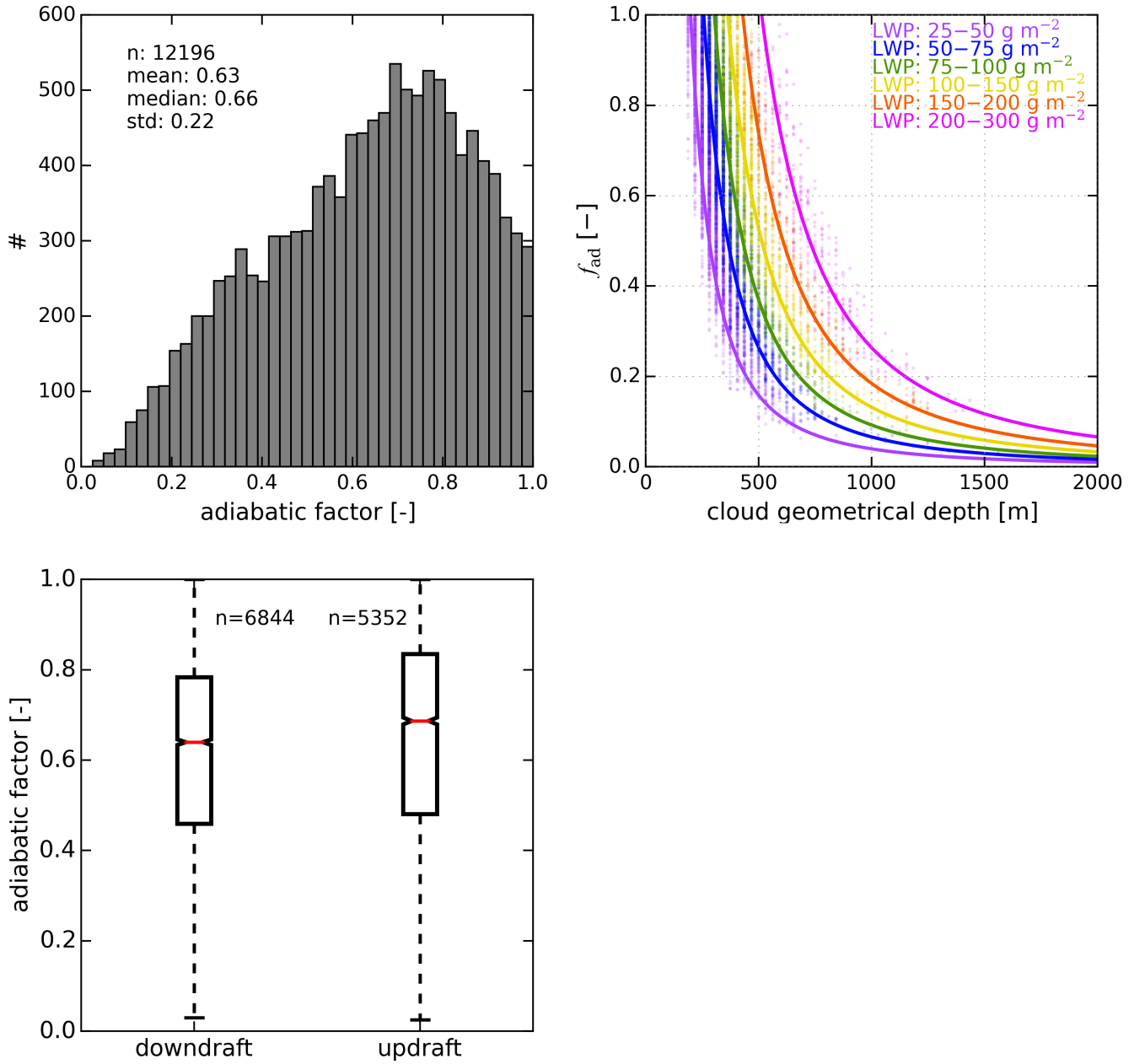
Figure 3. (a) Histogram of the adiabatic factor in 2012 and 2013 at LACROS. (b) Adiabatic factor as a function of observed cloud geometrical depth. Colors indicate different liquid water path bins. The solid lines represent the relationship described in Eq. (2) for bin mean liquid water path and $\Gamma_{ad} = 1.9 \cdot 10^{-3} \text{gm}^{-4}$. (c) Adiabatic factor seperated by up- and downdraft at the cloud base.

King, N. J., Bower, K. N., Crosier, J., and Crawford, I.: Evaluating MODIS cloud retrievals with in situ observations from VOCALS-REx, Atmospheric Chemistry and Physics, 13, 191–209, doi:10.5194/acp-13-191-2013, 2013.

Krzywinski, M. and Altman, N.: Points of Significance: Visualizing samples with box plots, Nat Meth, 11, 119–120, 2014.

Lehmann, K., Siebert, H., and Shaw, R. A.: Homogeneous and Inhomogeneous Mixing in Cumulus Clouds: Dependence on Local Turbulence Structure, Journal of the Atmospheric Sciences, 66, 3641–3659, doi:10.1175/2009JAS3012.1, 2009.

Loeb, N. G. and Coakley, J. A.: Inference of Marine Stratus Cloud Optical Depths from Satellite Measurements: Does 1D Theory
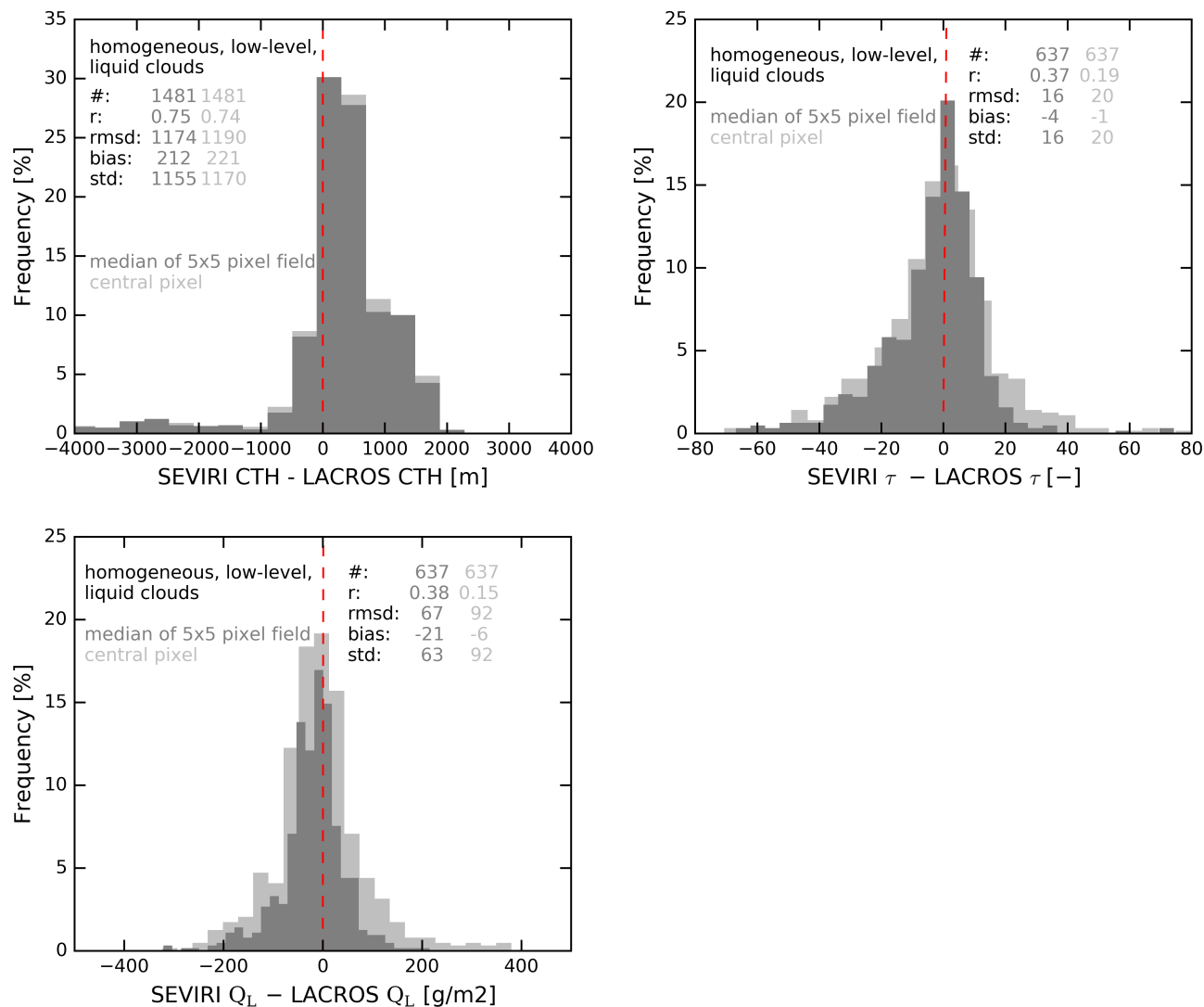
Figure 4. Histogram of differences between SEVIRI and LACROS derived cloud properties for 2012 and 2013: (a) cloud top height (CTH), (b) cloud optical depth (τ), (c) liquid water path (Q_L). Median of 5x5 SEVIRI pixels centered at LACROS (dark gray), closest pixel to LACROS (light gray). Zero difference is marked by a dashed red line.

Table 6. Mean difference of cloud optical depth between SEVIRI and LACROS for each case, when the adiabatic factor as obtained from the ground-based observations is applied and the adiabatic factor is considered constantly 1.

Date	$\overline{\tau_{\mathrm{SEVIRI}} - \tau_{\mathrm{LACROS}}}\left(f_{\mathrm{ad}} = f_{\mathrm{ad}}^{\mathrm{LACROS}}\right)$	$\overline{\tau_{\mathrm{SEVIRI}} - \tau_{\mathrm{LACROS}}}(f_{\mathrm{ad}} = 1)$
21 Apr 2013	2.3	8.5
27 Oct 2011	3.6	6.6
27 Sep 2012	7.9	10.9
01 Jun 2012	9.3	12.8

Apply?, Journal of Climate, 11, 215–233, doi:10.1175/1520-0442(1998)011<0215:IOMSCO>2.0.CO;2, 1998.

Löhnert, U., Crewell, S., Simmer, C., and Macke, A.: Profiling Cloud Liquid Water by Combining Active and Passive Mi-crowave Measurements with Cloud Model Statistics, Journal of Atmospheric and Oceanic Technology, 18, 1354–1366, doi:10.1175/1520-0426(2001)018<1354:PCLWBC>2.0.CO;2, 2001.
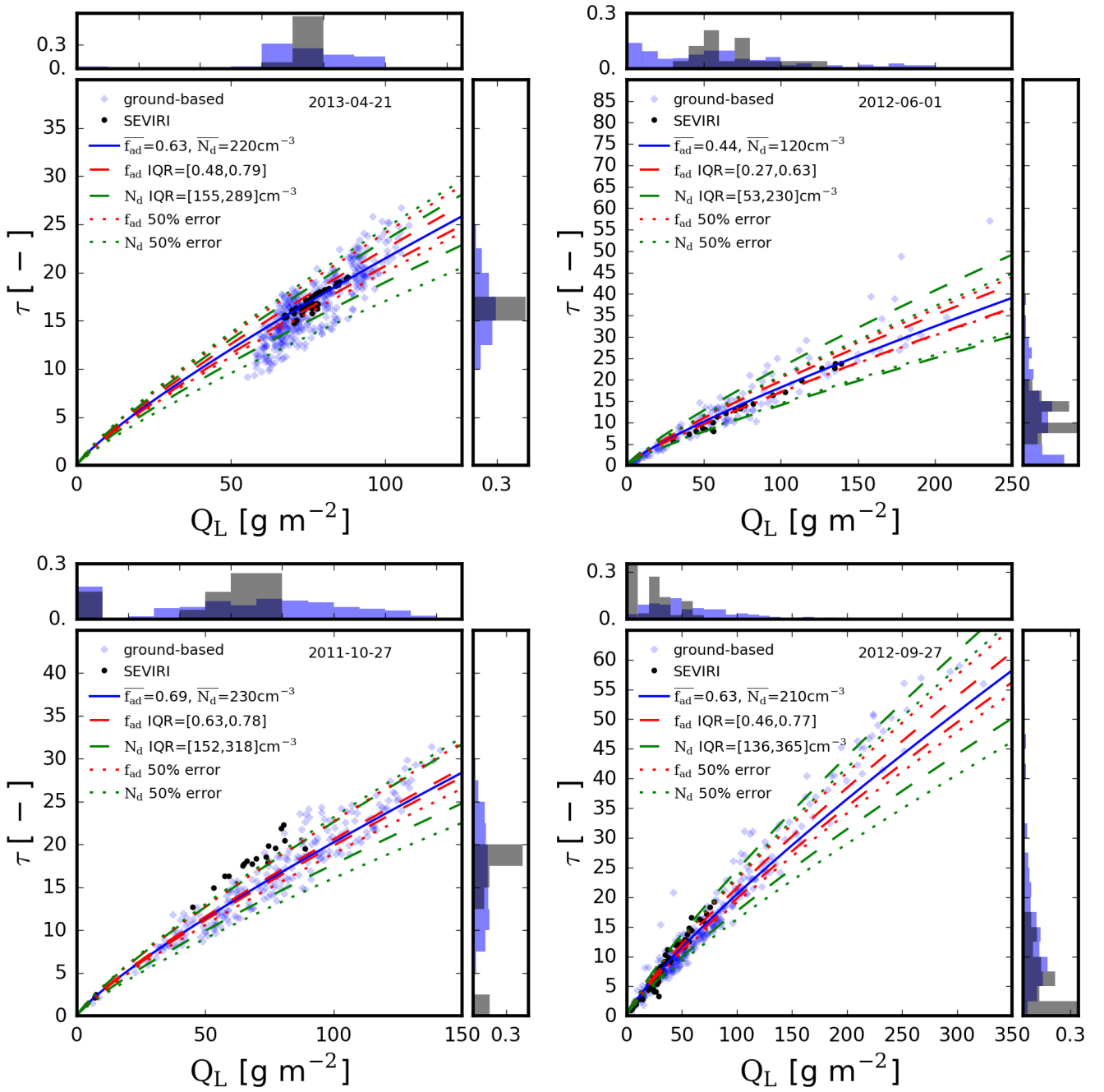
Figure 5. Relationship between liquid water path Q_L and optical depth τ for the four case days (Table 2). Blue crosses represent the LACROS observations for the case day, black dots the SEVIRI observations. The solid blue line represents the relationship between τ and Q_L for the median f_{ad} and N_d of the LACROS observations. Uncertainty estimates of τ as a function of Q_L is given in terms of temporal variability using the interquartile range (IQR) of the time-series (dashed), and as 50% relative uncertainty in N_d and f_{ad} (dotted). Furthermore the histograms of ground-based and SEVIRI observations are shown on each axis in the same colors as stated before.

Löhnert, U., Feingold, G., Uttal, T., Frisch, A. S., and Shupe, M. D.: Analysis of two independent methods for retrieving liquid water profiles in spring and summer Arctic boundary clouds, Journal of Geophysical Research: Atmospheres, 108, n/a–n/a, doi:10.1029/2002JD002861, 2003.

Mace, G. G. and Sassen, K.: A constrained algorithm for retrieval of stratocumulus cloud properties using solar radiation, microwave radiometer, and millimeter cloud radar data, Journal of Geophysical Research: Atmospheres, 105, 29 099–29 108, doi:10.1029/2000JD900403, 2000.
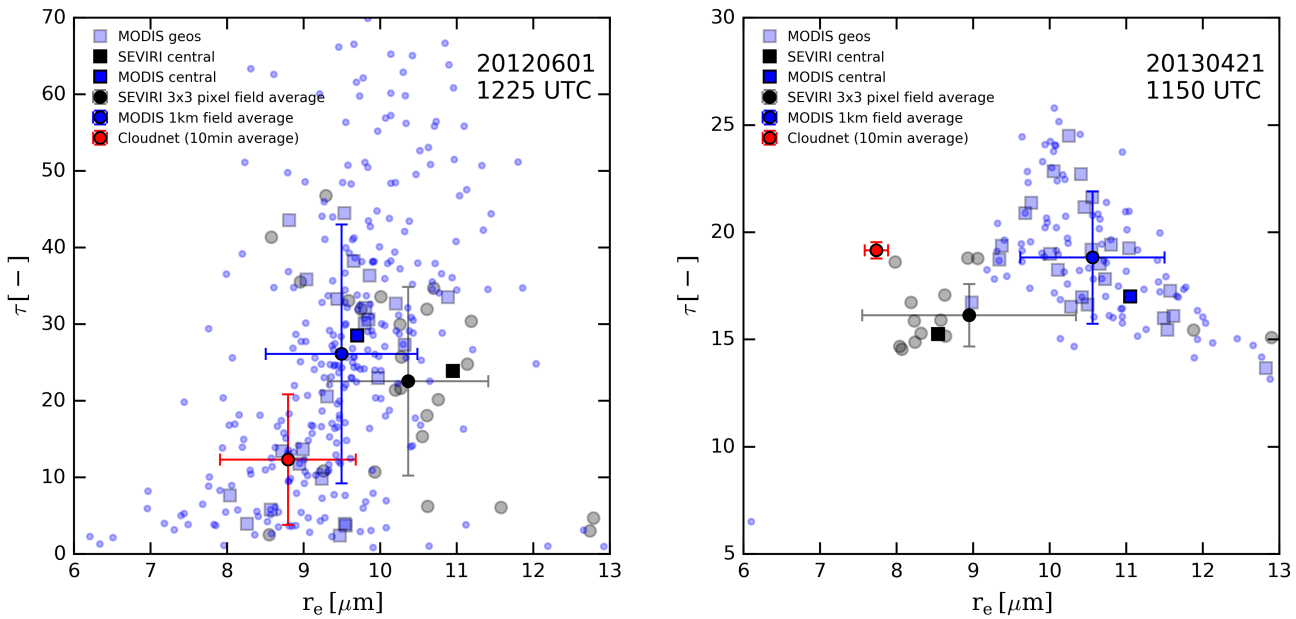
Figure 6. Effect of spatial resolution by comparing MODIS and SEVIRI observations for two timesteps: (a) inhomogeneous case, 1 June 2012 at 12:25 UTC, (b) homogeneous case, 21 April 2013 at 11:50 UTC. SEVIRI values are shown in black, MODIS values in blue and ground-based ones in red. The closest pixel (central) to LACROS is shown as a dark square. Field averages from the sensors original resolution are given as dots. For MODIS also the average to SEVIRI resolution is presented (MODIS geos, light blue square). Also the standard deviation is shown together with the averages in terms of error bars.

Marshak, A., Platnick, S., Várnai, T., Wen, G., and Cahalan, R. F.: Impact of three-dimensional radiative effects on satellite retrievals of cloud droplet sizes, Journal of Geophysical Research: Atmospheres, 111, n/a–n/a, doi:10.1029/2005JD006686, d09207, 2006.

Martin, G. M., Johnson, D. W., and Spice, A.: The Measurement and Parameterization of Effective Radius of Droplets in Warm Stratocumulus Clouds, Journal of the Atmospheric Sciences, 51, 1823–1842, doi:10.1175/1520-0469(1994)051<1823:TMAPOE>2.0.CO;2, 1994.

Martucci, G. and O'Dowd, C. D.: Ground-based retrieval of continental and marine warm cloud microphysics, Atmospheric Measurement Techniques, 4, 2749–2765, doi:10.5194/amt-4-2749-2011, 2011.

Martucci, G., Milroy, C., and O'Dowd, C. D.: Detection of Cloud-Base Height Using Jenoptik CHM15K and Vaisala CL31 Ceilometers, Journal of Atmospheric and Oceanic Technology, 27, 305–318, doi:10.1175/2009JTECHA1326.1, 2010.

McComiskey, A. and Feingold, G.: The scale problem in quantifying aerosol indirect effects, Atmospheric Chemistry and Physics, 12, 1031–1049, doi:10.5194/acp-12-1031-2012, 2012.

Meerkötter, R. and Bugliaro, L.: Diurnal evolution of cloud base heights in convective cloud fields from MSG/SEVIRI data, Atmospheric Chemistry and Physics, 9, 1767–1778, doi:10.5194/acp-9-1767-2009, 2009.

Meerkötter, R. and Zinner, T.: Satellite remote sensing of cloud base height for convective cloud fields: A case study, Geophysical Research Letters, 34, n/a–n/a, doi:10.1029/2007GL030347, 2007.

Miles, N. L., Verlinde, J., and Clothiaux, E. E.: Cloud Droplet Size Distributions in Low-Level Stratiform Clouds, Journal of the Atmospheric Sciences, 57, 295–311, doi:10.1175/1520-0469(2000)057<0295:CDSDIL>2.0.CO;2, 2000.

Miller, M. A., Jensen, M. P., and Clothiaux, E. E.: Diurnal Cloud and Thermodynamic Variations in the Stratocumulus Transition Regime: A Case Study Using In Situ and Remote Sensors, Journal of the Atmospheric Sciences, 55, 2294–2310, doi:10.1175/1520-0469(1998)055<2294:DCATVI>2.0.CO;2, 1998.

Min, Q. and Duan, M.: Simultaneously retrieving cloud optical depth and effective radius for optically thin clouds, Journal of Geophysical Research: Atmospheres, 110, n/a–n/a, doi:10.1029/2005JD006136, d21201, 2005.

Min, Q., Joseph, E., Lin, Y., Min, L., Yin, B., Daum, P. H., Kleinman, L. I., Wang, J., and Lee, Y.-N.: Comparison of MODIS cloud microphysical properties with in-situ measurements over the Southeast Pacific, Atmospheric Chemistry and Physics, 12, 11 261–11 273, doi:10.5194/acp-12-11261-2012, 2012.

Nakajima, T. and King, M. D.: Determination of the Optical Thickness and Effective Particle Radius of Clouds from Reflected Solar Radiation Measurements. Part I: Theory, Journal of the Atmospheric Sciences, 47, 1878–1893, doi:10.1175/1520-0469(1990)047<1878:DOTOTA>2.0.CO;2, 1990.

Painemal, D. and Zuidema, P.: Microphysical variability in southeast Pacific Stratocumulus clouds: synoptic conditions and radiative response, Atmospheric Chemistry and Physics, 10, 6255–6269, doi:10.5194/acp-10-6255-2010, 2010.

Painemal, D. and Zuidema, P.: Assessment of MODIS cloud effective radius and optical thickness retrievals over the Southeast Pacific with VOCALS-REx in situ measurements, Journal of Geophysical Research: Atmospheres, 116, n/a–n/a, doi:10.1029/2011JD016155, 2011.

Pawlowska, H., Brenguier, J., and Burnet, F.: Microphysical properties of stratocumulus clouds, Atmospheric Research, 55, 15 – 33, doi:http://dx.doi.org/10.1016/S0169-8095(00)00054-5, 2000.

Pawlowska, H., Grabowski, W. W., and Brenguier, J.-L.: Observations of the width of cloud droplet spectra in stratocumulus, Geophysical Research Letters, 33, n/a–n/a, doi:10.1029/2006GL026841, 119810, 2006.

Petty, G. W. and Huang, W.: The Modified Gamma Size Distribution Applied to Inhomogeneous and Nonspherical Particles: Key Relationships and Conversions, Journal of the Atmospheric Sciences, 68, 1460–1473, doi:10.1175/2011JAS3645.1, 2011.

Platnick, S.: Vertical photon transport in cloud remote sensing problems, Journal of Geophysical Research: Atmospheres, 105, 22 919–22 935, doi:10.1029/2000JD900333, 2000.

Platnick, S. and Valero, F. P. J.: A Validation of a Satellite Cloud Retrieval during ASTEX, Journal of the Atmospheric Sciences, 52, 2985–3001, doi:10.1175/1520-0469(1995)052<2985:AVOASC>2.0.CO;2, 1995.

Platnick, S., King, M. D., Ackerman, S. A., Menzel, W. P., Baum, B. A., Riédi, J. C., and Frey, R. A.: The MODIS cloud products: Algorithms and examples from Terra, Geoscience and Remote Sensing, IEEE Transactions on, 41, 459–473, 2003.

Quaas, J., Boucher, O., and Lohmann, U.: Constraining the total aerosol indirect effect in the LMDZ and ECHAM4 GCMs using MODIS satellite data, Atmospheric Chemistry and Physics, 6, 955, 2006.

Rémillard, J., Kollias, P., and Szyrmer, W.: Radar-radiometer retrievals of cloud number concentration and dispersion parameter in nondrizzling marine stratocumulus, Atmospheric Measurement Techniques, 6, 1817–1828, doi:10.5194/amt-6-1817-2013, 2013.

Roebeling, R., Placidi, S., Donovan, D., Russchenberg, H., and Feijt, A.: Validation of liquid cloud property retrievals from SEVIRI using ground-based observations, Geophysical Research Letters, 35, L05 814, 2008a.

Roebeling, R. A., Feijt, A. J., and Stammes, P.: Cloud property retrievals for climate monitoring: Implications of differences between Spinning Enhanced Visible and Infrared Imager (SEVIRI) on METEOSAT-8 and Advanced Very High Resolution Radiometer (AVHRR) on NOAA-17, Journal of Geophysical Research: Atmospheres, 111, n/a–n/a, doi:10.1029/2005JD006990, 2006.

Roebeling, R. A., Deneke, H. M., and Feijt, A. J.: Validation of Cloud Liquid Water Path Retrievals from SEVIRI Using One Year of CloudNET Observations, Journal of Applied Meteorology and Climatology, 47, 206–222, doi:10.1175/2007JAMC1661.1, 2008b.

Rosenfeld, D., Wang, H., and Rasch, P. J.: The roles of cloud drop effective radius and LWP in determining rain proper-ties in marine stratocumulus, Geophysical Research Letters, 39, doi:10.1029/2012GL052028, 2012.

Saunders, R., Matricardi, M., and Brunel, P.: An improved fast radiative transfer model for assimilation of satellite radiance observations, Quarterly Journal of the Royal Meteorological Society, 125, 1407–1425, doi:10.1002/qj.1999.49712555615, 1999.

Schmetz, J., Pili, P., Tjemkes, S., Just, D., Kerkmann, J., Rota, S., and Ratier, A.: An introduction to Meteosat Second Generation (MSG)., Bulletin of the American Meteorological Society, 83, 2002.

Schmidt, J., Ansmann, A., Bühl, J., Baars, H., Wandinger, U., Müller, D., and Malinka, A. V.: Dual-FOV Raman and Doppler lidar studies of aerosol-cloud interactions: Simultaneous profiling of aerosols, warm-cloud properties, and vertical wind, Journal of Geophysical Research: Atmospheres, 119, 5512–5527, doi:10.1002/2013JD020424, 2014.

Schueller, L., Brenguier, J.-L., and Pawlowska, H.: Retrieval of microphysical, geometrical, and radiative properties of marine stratocumulus from remote sensing, J. Geophys. Res., 108, 8631, doi:10.1029/2002JD002680, 2003.

Schüller, L., Bennartz, R., Fischer, J., and Brenguier, J.-L.: An Algorithm for the Retrieval of Droplet Number Concentration and Geometrical Thickness of Stratiform Marine Boundary Layer Clouds Applied to MODIS Radiometric Observations, Journal of Applied Meteorology, 44, 28–38, doi:10.1175/JAM-2185.1, 2005.

Schulz, J., Albert, P., Behr, H.-D., Caprion, D., Deneke, H., Dewitte, S., Dürr, B., Fuchs, P., Gratzki, A., Hechler, P., Hollmann, R., Johnston, S., Karlsson, K.-G., Manninen, T., Müller, R., Reuter, M., Riihelä, A., Roebeling, R., Selbach, N., Tetzlaff, A., Thomas, W., Werscheck, M., Wolters, E., and Zelenka, A.: Operational climate monitoring from space: the EUMETSAT Satellite Application Facility on Climate Monitoring (CM-SAF), Atmospheric Chemistry and Physics, 9, 1687–1709, doi:10.5194/acp-9-1687-2009, 2009.

Shupe, M. D.: A ground-based multisensor cloud phase classifier, Geophysical Research Letters, 34, n/a–n/a, doi:10.1029/2007GL031008, 2007.

Stephens, G. L., Vane, D. G., Boain, R. J., Mace, G. G., Sassen, K., Wang, Z., Illingworth, A. J., O'Connor, E. J., Rossow, W. B., Durden, S. L., Miller, S. D., Austin, R. T., Benedetti, A., Mitrescu, C., and CloudSat Science Team, T.: THE CLOUDSAT MISSION AND THE A-TRAIN, Bulletin of the American Meteorological Society, 83, 1771–1790, doi:10.1175/BAMS-83-12-1771, 2002.

Stuhlmann, R., Rodriguez, A., Tjemkes, S., Grandell, J., Arriaga, A., Bézy, J.-L., Aminou, D., and Bensi, P.: Plans for EUMETSAT's Third Generation Meteosat geostationary satellite programme, Advances in Space Research, 36, 975 – 981, doi:http://dx.doi.org/10.1016/j.asr.2005.03.091, atmospheric Remote Sensing: Earth's Surface, Troposphere, Stratosphere and Mesosphere- I, 2005.

Szczodrak, M., Austin, P. H., and Krummel, P. B.: Variability of Optical Depth and Effective Radius in Marine Stratocumulus Clouds, Journal of the Atmospheric Sciences, 58, 2912–2926, doi:10.1175/1520-0469(2001)058<2912:VOODAE>2.0.CO;2, 2001.

Turner, D. D., Vogelmann, A. M., Johnson, K., Miller, M., Austin, R. T., Barnard, J. C., Flynn, C., Long, C., McFarlane, S. A.,

Cady-Pereira, K., Clough, S. A., Chiu, J. C., Khaiyer, M. M., Liljegren, J., Lin, B., Minnis, P., Marshak, A., Matrosov, S. Y., Min, Q., O'Hirok, W., Wang, Z., and Wiscombe, W.: Thin Liquid Water Clouds: Their Importance and Our Challenge, Bulletin of the American Meteorological Society, 88, 177–190, doi:10.1175/BAMS-88-2-177, 2007.

Twomey, S.: Pollution and the planetary albedo, Atmospheric Environment (1967), 8, 1251 – 1256, doi:10.1016/0004-6981(74)90004-3, 1974.

Wang, L., Qu, J. J., Xiong, X., Hao, X., Xie, Y., and Che, N.: A New Method for Retrieving Band 6 of Aqua MODIS, IEEE GEOSCIENCE AND REMOTE SENSING LETTERS, 3, 267, 2006.

Warner, J.: The Water Content of Cumuliform Cloud, Tellus, 7, 449–457, doi:10.1111/j.2153-3490.1955.tb01183.x, 1955.

Winker, D. M., Vaughan, M. A., Omar, A., Hu, Y., Powell, K. A., Liu, Z., Hunt, W. H., and Young, S. A.: Overview of the CALIPSO Mission and CALIOP Data Processing Algorithms, Journal of Atmospheric and Oceanic Technology, 26, 2310–2323, doi:10.1175/2009JTECHA1281.1, 2009.

Wood, R.: Relationships between optical depth, liquid water path, droplet concentration, and effective radius in adiabatic layer cloud, University of Washington, 3, 2006.

Yang, Y., Marshak, A., Mao, J., Lyapustin, A., and Herman, J.: A method of retrieving cloud top height and cloud geometrical thickness with oxygen A and B bands for the Deep Space Climate Observatory (DSCOVR) mission: Radiative transfer simulations, Journal of Quantitative Spectroscopy and Radiative Transfer, 122, 141 – 149, doi:http://dx.doi.org/10.1016/j.jqsrt.2012.09.017, {INTERNATIONAL} {SYMPOSIUM} {ON} {ATMOSPHERIC} {LIGHT} {SCATTERING} {AND} {REMOTE} {SENSING} (ISALSaRS'11), 2013.

Zeng, S., Riedi, J., Trepte, C. R., Winker, D. M., and Hu, Y.-X.: Study of global cloud droplet number concentration with A-Train satellites, Atmospheric Chemistry and Physics, 14, 7125–7134, doi:10.5194/acp-14-7125-2014, 2014.

Zinner, T. and Mayer, B.: Remote sensing of stratocumulus clouds: Uncertainties and biases due to inhomogeneity, J. Geophys. Res., 111, D14 209, doi:10.1029/2005JD006955, 2006.